Development of Safe and Efficient Operation for an Airborne Wind Energy (AWE) System - A Rotary Design

Second Year Review

Oliver Tulloch
Registration Number: 201574526

Wind and Marine Energy Systems Centre for Doctoral Training
Department of Electronic and Electrical Engineering
University of Strathclyde, Glasgow

April 1, 2019

This report is the result of the author's original research. It has been composed by the author and has not been previously submitted for examination which has led to the award of a degree.

Abstract

This report details the work that has been done in the 2nd year of a 3 year research PhD. A brief background into the motivation behind this work is given along with an introduction to Airborne Wind Energy. The novelty of this work is described and the aims and objectives of this research are set out. A short literature review is then given highlighting the prior research on the modelling of airborne wind energy systems with a particular focus on rotary system. Following this rotary systems are defined and the existing prototypes are introduced. A test campaign run on the Daisy Kite design is then described with the results collected so far shown. Finally a mathematical model is introduced. The model is used to simulate the Daisy Kite and its results are compared to the experimental data collected during the test campaign. It is shown the model is able to accurately predicted the Daisy Kites power output. This report is concluded by highlighting the future work that will initially focus on the development of a dynamic model of the tensile rotary power transmission used within the Daisy Kite.

Contents

List of Figures

List of Tables

Nomenclature

Acronyms

AWE	Airborne Wind Energy	
AWES	Airborne Wind Energy Systems	
BEM	Blade Element Momentum	
HAWT	Horizontal Axis Wind Turbine	
LCOE	Levelised Cost of Energy	
LTA	Lighter Than Air	
TRPT	Tensile Rotary Power Transmission	
VESC	Vedder Electronic Stability Controller	

Symbols

ω	Rotational speed	rad/s
ρ	Air density	kg/m^3
ζ	Power harvesting factor	
A	Area	m^2
C_D	Drag coefficient	
C_L	Lift coefficient	

C_P	Power coefficient	
C_{TDE}	Tether Drag Equivalent Coefficient	
D	Drag force	N
I	Current	A
K	Torsional stiffness	Nm/rad
L	Lift force	N
P	Power	W
Q	Torque	Nm
S	Wing area	m^2
T	Tension	N
U	Wind speed	m/s
V	Voltage	V

"The use of means never before heard of for the doing of things never before done, cannot fail to excite considerable interest; and the more especially so if the objects accomplished wear any features of public utility"

GEORGE POCOCK
THE AEROPLEUSTIC ART

Chapter 1

Introduction

This report details the progress that has been made in the 2nd year of a 3 year research PhD on the development of Airborne Wind Energy (AWE) systems.

1.1 Motivation of Research

The wind energy sector continues to grow year on year. A global wind energy capacity of 539GW had been installed by the end of 2017, an increase of 11% from 2016 [8]. As turbine size increases and costs continue to fall wind energy is becoming more and more competitive in the global market. The wind industry has relied on the three bladed Horizontal Axis Wind Turbines (HAWT) for these achievements. Airborne wind energy is a form of wind power where energy is harnessed using tethered wings. It is envisaged that AWE will reduce the cost of wind energy and be able to access locations where it is currently not feasible to install HAWT. Diehl [9, Chapter 1] highlights three key reasons why research into AWE continues:

1. The amount of energy contained within the wind
2. The altitude at which much of the wind resource is located
3. The potential low mass and cost per unit of usable power

One of the biggest advantages of Airborne Wind Energy Systems (AWES) over conventional HAWT is the ability of a AWES to alter the airspace in which it operates. This gives AWE devices more flexibility around their operating environment which in turn helps to maximise their power output.

1.1.1 Resource Analysis

As highlighted by Diehl [9, Chapter 1] one of the drivers for research into AWE is the ability of a tethered wing to reach much higher altitudes compared to HAWT and that there is more wind power available at higher altitudes. As discussed by Archer [10] the wind power per unit area, or the wind power density, generally increases with altitude. Within the planetary boundary layer the increase in wind speed can be said to follow a log-law as defined in (1.1) where V_{ref} is a reference wind speed at a reference altitude Z_{ref}, Z_0 is the surface roughness and V_Z is the wind speed at altitude Z. The height of the boundary layer can vary greatly depending on location and time. Boundary layer heights can range form 100m to 2km.

$$V_z = V_{ref} \frac{ln\frac{Z}{Z_0}}{ln\frac{Z_{ref}}{Z_0}} \tag{1.1}$$

Above the boundary layer much less is known and understood about the variation in wind power density. Archer shows that the greatest wind power density is between 8 - 10km above the Earth's surface. However, most AWES today target much lower altitudes of between 100 - 500m. This is because in general the greatest increases in wind speed with height occur within the boundary layer. Therefore by operating at altitudes just outside the planetary boundary layer AWES accesses greater wind power densities than current HAWT are able to. Tether drag dominates the aerodynamic drag for many AWES [9, Chapter 1]. Therefore most systems aim to avoid very long tether lengths. This is also a key reason why most AWE concepts aim for maximum altitudes of around 500m.

As highlighted by Archer wind power density not only varies with altitude but also with location and time. HAWT are restricted to operating in the same airspace at all times. However, the use of tethered wings allows AWES to alter their operational height and therefore the airspace that they operate in. It is possible for an AWES to always operate in the air space with the highest wind power density within the systems physical constraints. Bechtle [11] shows the potential energy yield for an AWES that operates at this optimal altitude for locations in Europe. The ability to change its operational height could also be used as a method of controlling a devices power output at above rated wind speeds. If AWES are to be deployed on even moderate scales much more research is required into the wind resource at altitudes up to 500m.

Fagiano [12] and Cherubini [13] both give overviews of the AWE industry. Fagiano introduces the basics behind AWE while Cherubini introduces the main categories of AWES and gives an overview of current concepts under development. A brief up to date overview of the AWE industry is presented below.

1.1.2 Classification of AWE Systems

With over 60 organisations worldwide actively involved in the development of AWE there are a large number of different concepts that have been proposed [14]. With so many different concepts it is useful to group devices that share similarities. This makes the comparison of different systems more simple. It also allows for the identification of any trends within the industry.

Fly-Gen or Ground-Gen

All AWES fall into one of two categories when it comes to the location at which electricity is generated. This can either be done in the air, Fly-Gen, or at a ground station, Ground-Gen. Fly-Gen devices have a large disadvantage when it comes to weight. Generators are heavy and Fly-Gen devices must mount them on the airborne components.

This not only increases their weight but also their complexity. However, many Fly-Gen systems use rotors for power extracting. These rotors can be used to power the devices. This allows for more controlled launch and landing procedures and for the device to remain airborne during short periods when the wind speed drops below the systems cut-in wind speed. Ground-Gen systems have more simple lighter wings but launch and landing procedures are often more challenging.

All AWES must somehow transmit the power that is harnessed aloft down to the ground. The choice of generator location dictates the method of power transmission. It can either be done electrically for Fly-Gen systems or mechanically for Ground-Gen systems. The need for the tether to conduct electricity for Fly-Gen systems results in a larger diameter tether which will increase the tether drag and decrease the systems efficiency. There are many methods that have been proposed to mechanically transmit the power to the ground for Ground-Gen systems. The most developed uses the tension in the tether to pull the tether off a winch and turn a generator at the ground station. This does mean that when the end of the tether is reached it must be reeled back in, consuming some of the power that has just been generated. It also means that the system cannot generate power continuously. This method is often referred to as pumping cycle or yo-yo generation.

Rigid Wing or Soft Wing

Another key difference between AWES is the structure of the airborne components or wings that are used. They can either be rigid or soft. A rigid wing has a solid structure much like an airplane wing or wind turbine blade. A soft wing has a flexible structure similar to a sport kite or parachute. Rigid wings are much more aerodynamically efficient which results in a greater power output. There is also a vast amount of knowledge around how they react within the airflow from the aerospace industry. This makes modelling rigid wings more straight forward and more reliable which results in better predictions of movement and therefore more accurate control. However, they tend to

be heavier and more fragile. By comparison soft wings are much more lightweight and robust. As systems are increasing in size there appears to be a trend to move towards rigid wings. This is down to the better aerodynamic efficiency and their predictability.

Multi Wing Systems

There are a number of AWES that use several wings networked together. This can often result in a reduction in overall tether drag as there can be less tether length for a given kite area. The wings can also be flown such that large sections of the tethers are kept stationary within the air. They also offer a certain amount of redundancy to the system. Rotary AWES are a subset of multi wing systems. Rotary AWES use networks of wings that form rotors similar to that of a HAWT. The biggest advantage of rotary AWES is that they often need less and even no active control to keep the wings on the desired flight path.

Lighter then Air

A standalone category of AWE are Lighter Than Air (LTA) systems. These rely on aerostatic lift instead of aerodynamic lift to remain airborne. LTA devices have large shrouds full of a lighter than air gas such as Helium. This gives them enough buoyancy to remain airborne whatever the wind conditions. There are clear advantageous around launch, landing and periods of low wind for LTA devices. However, the large shroud results in very poor lift to drag ratios. This is particularly important when higher wind speeds are encountered and makes it difficult for LTA systems to achieve larger sizes.

1.1.3 Current AWE Leaders

Although there are a large number of organisations involved in AWE none have achieved commercial deployment. There are a number of companies that are getting closer with products predicted to be made available in the early to mid 2020's.

At present the largest prototype that has been built and tested is Makani's 600kW Fly-Gen system [15]. Their system uses a 26m rigid wing with 8 rotors mounted on it. Makani has recently graduated from X, Alphabet's incubator for technology start-up's, to become an independent company. This followed an announcement that Royal Dutch Shell have invested in Makani and are collaborating on a offshore test site in Norway [16]. Makani appear to have the most developed system and seem to be the closest to achieving commercialisation.

Glasgow based Kite Power Systems (KPS) are developing a dual kite pumping cycle system. To combat the non-continuous power from a pumping cycle kite KPS use two kites in anti-phase [17]. As one kite is pulling the tether out and generating power the other is being reeled back in. Through the use of a hydraulic power take off the power output from the whole system is kept more constant. They are currently manufacturing a 500kW prototype.

Ampyx power have developed a rigid wing pumping cycle system. With a number of prototypes already constructed and tested they are currently manufacturing AP3 a 300kW system. The aim of AP3 is to demonstrate launch and landing operations along with safe and autonomous operation [18]. Upon a successful testing campaign using AP3, Ampyx plan to design and built a 2MW system for commercial deployment.

1.2 Novelty of Research

It is envisaged that by using less material and accessing harder to reach locations AWE will reduce the cost of wind energy. As a relatively new area of research there are a great number of AWES designs and concepts. A sector of AWES that has received very little research attention is that of rotary AWES. Rotary AWES are systems that use multiple wings networked together were the wings form a rotor similar to that of a HAWT [19] [20] [3, Chapters 21 & 22]. Their development has mostly been driven

through trial and error by individuals. Within rotary AWES the power transmission from the airborne rotor down to the ground station is not well understood, in particular the mechanical form termed tensile rotary power transmission (TRPT). It is likely that the size that TRPT can achieve will limit the size of the rotary concepts that use it. Therefore by expanding the knowledge of such a power transmission system the scalability of rotary AWES can be assessed and their designs refined. At present control methods for rotary AWES are focused on survivability [21, 22]. By increasing the knowledge around these designs it will be possible to improve their control. In-particular operational control that is able to maximise the power output in the uncertain environment encountered by AWES.

1.3 Aims and Objectives

1.3.1 Aim

To understand and develop rotary AWE through modelling and control techniques, with a focus on assessing the scalability and feasible operational strategies.

1.3.2 Objectives

1. Development of a mathematical model - To better understand the working principles of rotary AWES a working mathematical model will be produced. This model will be based on the Daisy Kite developed by Windswept and Interesting [21]. Simulations using this model will then be used to improve and optimise the design of rotary AWES with respect to key design drivers e.g. power capture and cost.

2. Improved design and testing of a small-scale prototype - A small scale prototype will be designed, manufactured and tested. Empirical data will be obtained for model validation as there are no other AWE systems that are similar to rotary kite systems.

3. Investigate the scalability of rotary kite systems to industrial scale AWE - At present a small scale 500W system has been produced. The feasibility of a much larger system is unknown. For rotary kite systems to be a commercial success larger systems should be investigated. Using the developed mathematical model an assessment of rotary AWES scaling potential will be conducted.

4. Investigate control strategies to achieve safe and efficient operation - To optimise the design, it is necessary to consider how the device will operate in an uncertain environment. The mathematical model and small-scale prototype will be used to develop an operating strategy and the control system. Supervisory control to ensure that the system operates in a safe manner will also be explored.

This Chapter has introduced airborne wind energy and the aims and objectives for this research. The remainder of the report is structured as follows:

- Chapter 2 gives a brief literature review of the key prior research in relation to the modelling of rotary AWES. It also provides a detailed description of rotary AWES. Rotary systems that are currently under development are introduced followed by detailed descriptions of experimental tests conducted on the Daisy Kite.

- Chapter 3 details the mathematical model that has been developed for rotary AWES. Based on the Daisy Kite the model has been broken down into a series of modules. These modules are introduced and explained. The output from the mathematical model is compared to the experimental data.

- Chapter 4 concludes this report detailing the planned work for the final year of this PhD research.

Chapter 2

An Introduction to Rotary Airborne Wind Energy Systems

This Chapter introduces the background literature on AWE before focusing on rotary AWES. Several rotary designs with working prototypes are introduced before a series of test on one of these, the Daisy Kite, are detailed.

2.1 Literature Review - Methodology

This Section will introduce the currently available literature on the modelling of AWES with a focus on rotary systems. It is split into three sections. Section 2.1.1 looks at the modelling and analysis of AWES in general. Although this research focuses on rotary system it is important to understand the wider scope of AWES. So that a clear comparison between rotary AWES and other systems can be made. Section 2.1.2 deals with modelling of rotor aerodynamics while Section 2.1.3 focuses on tensile rotary power transmission.

2.1.1 Airborne Wind Energy Overview

It has been known for millennia that kites are able to perform useful work. There are accounts of them being used in ancient China to send signals, lift men to scout enemy troops and even to drop bombs [23]. However, it was not until the early 1980's that the function of energy generation by kite systems was analysed in any depth. The basic analysis of AWE was introduced by Loyd [24]. Loyd analysed the maximum energy that can be theoretically extracted by a tethered wing. He introduced three scenarios which he terms: simple kite, lift power and drag power. The simple kite refers to a stationary wing whereas the lift power and drag power scenarios utilise crosswind motion. Lift power refers to a system that uses the wings lift to generate power. For example an AWES that uses a pumping cycle is using lift power. Drag power refers to a system where drag is added to the wind to generate power. Makani's Fly-Gen system is an example of this as rotors are placed on the wing that increases the drag. Loyd shows that by flying a wing crosswind, thereby increasing the relative wind speed that the wing sees, the maximum theoretical power is greatly increased. This explaining why almost all AWES that are being developed today use crosswind motion. The maximum power that can be extracted by a tethered wing in either lift or drag power, as defined by Loyd, is given by (2.1) where P is power, ρ the air density, V_∞ the wind speed, A the wing area, C_L the wings lift coefficient and C_D the wings drag coefficient.

$$P = \frac{2}{27}\ \rho\ U_\infty^3\ A\ C_L\ \left(\frac{C_L}{C_D}\right)^2 \tag{2.1}$$

The drag on an AWES tether will be included into the calculation of the maximum theoretical power. To keep the analysis simple the tether drag is often added as an equivalent drag force acting on the wing [13, 25]. Therefore C_D in (2.1) is replaced by the wings drag coefficient plus the tether drag equivalent coefficient acting on the wing. This is shown by (2.2) where C_{TDE} is the tether drag equivalent coefficient [13].

$$P = \frac{2}{27}\ \rho\ U_{\infty}^{3}\ A\ C_L\ \left(\frac{C_L}{C_D + C_{TDE}}\right)^2 \tag{2.2}$$

A basic analysis shows that, particularly for aerodynamically efficient wings with high $\frac{C_L}{C_D}$, the tether drag will dominate the systems drag [9, Chapter 1]. It is therefore important to include the tether drag factor in the basic analysis of any AWES. Loyd's simple analyses with the addition of tether drag provides a useful upper limit for AWES that use lift power or drag power.

Loyd's analysis assumes that the wing is flying directly crosswind. In reality the wing flies at an angle that is similar to the elevation angle of the tether. This will result in a reduced power output compared to that calculated in (2.2). This can be accounted for by replacing U_{∞} in (2.2) with $U_{\infty}cos(\alpha)$ where α is the elevation angle of the tether [9, Chapter 1]. This results in a power loss proportional to $cos(\alpha)^3$. This is also used within the wind turbine industry to account for yaw misalignment between the the rotor and the wind direction [26]. It is therefore advantageous to keep the elevation angle low to minimise the power loses. However, this will result in longer tethers to reach the same operational altitude. As highlighted above for high efficiency wings the tether dominates the systems drag therefore shorter tethers are preferred.

Loyd's model gives a useful upper limit for lift or drag power AWES. The maximum power output, according to Loyd's analysis, is dictated by the lift and drag coefficients of the wing and tether. There is not yet an established theoretical upper limit for the maximum power for AWES. Within the wind turbine industry the proportion of available wind power that a turbine is able to extract from its swept area is defined as the power coefficient (C_P) as shown by (2.3) where A is the swept area of the rotor. A turbines power coefficient is a useful metric when comparing different turbines under different operating conditions.

$$C_P = \frac{P}{\frac{1}{2}\ \rho\ A\ U_\infty^3} \tag{2.3}$$

The maximum power coefficient that can be achieved by a turbine is known as the Betz limit after the German aerodynamics Albert Betz [26]. Betz showed the maximum power coefficient to be $\frac{16}{27}$. This is widely accepted as the upper limit for any wind turbine. The Betz limit is based on linear momentum theory and a similar analysis has been applied to AWE [27, 28]. For drag power it is shown that the limit is $\frac{16}{27}$ exactly the same as a HAWT whereas for lift power the limit becomes $\frac{4}{27}$. The lower limit for lift power is due to the need for the wing to fly downwind so that the tether is pulled off a drum. Although the Betz limit is the maximum power ratio that can be extracted from a given cross sectional area it may not be a useful upper limit for many AWES. As the swept area of many AWES is very large their power coefficients are likely to be much lower than HAWT. Unlike HAWT it is also possible for multiple AWE devices to operate in the same airspace. The power coefficient of many AWES, especially those that use lift and drag power, is therefore not a useful comparison metric. It should be noted that there are some AWES that are more comparable to HAWT, like Altaeros's buoyant airborne turbine system [29]. The power coefficient and Betz limit are useful metrics for such devices but not for all other AWES. To compare general AWES another metric is needed.

A metric that is used for AWES is the power harvesting factor (ζ) . Very similar to the power coefficient it is defined as the power extracted by a wing compared to the wind power available within the wing area as shown by (2.4), where S is the wing area.

$$\zeta = \frac{P}{\frac{1}{2}\ \rho\ S\ U_\infty^3} = \frac{4}{27}\ C_L\ \left(\frac{C_L}{C_D}\right)^2 \tag{2.4}$$

The AWE company Makani have achieved a power harvesting factor of 8 [9, Chapter

28], modern HAWTs have a ζ of around 5.5 [9, Chapter 1]. For a rigid wing a ζ of 30 may be possible whereas for a soft wing the value will be much lower with a ζ of 4 potentially achievable. The power harvesting factor acts as a useful metric when comparing different AWES.

Ultimately AWES will be judged on the levelised cost of energy (LCOE) . This is the total cost of producing, installing and running the device divided by the energy it produces. Offshore wind achieved a strike price of £57.50/MWh in the most recent contracts for difference allocation round run by the UK government [30]. The projects that achieved this are due to begin operation in 2022/23, around the time that many AWE companies envisage entering the market with larger scale commercial systems [17, 18]. The day ahead wholesale price for electricity in the UK has historically been around £50/MWh [31]. This shows that wind energy is becoming much more competitive and what AWE will need to achieve if it is to reach large scale commercial deployment. It is predicted that AWE could reach a LCOE of £30/MWh by 2030 [32]. A study by BVG Associates on Kite Power Systems device has predicted a cost of $50/MWh in 2030 [33].

2.1.2 Rotors

Many AWES utilise rotors for energy extraction. These can be very similar to the rotors used by HAWT. The rotor used in Altaeros 30kW buoyant airborne turbine prototype was a standard wind turbine rotor. There are a number of analysis tools used for wind turbine rotors. The most basic of these is an actuator disc. In this case the rotor is modelled as a flat disc, as energy passes through the disc some of it is extracted [26, Chapter 3]. The power output is estimated by using the power coefficient as introduced previously and shown in (2.5).

$$P = \frac{1}{2}\ \rho\ A\ U_{\infty}^{3}\ cos(\alpha)^{3}\ C_P \tag{2.5}$$

The actuator disc can also be used to estimate the overall torque and thrust loads on the rotor given the thrust and torque coefficients. Actuator disc theory has the advantage of being very simple and therefore quick to apply and provide rough values for power, torque and thrust from a rotor. Key for a number of AWES this method can account for any misalignment between the wind direction and the rotors axis of rotation by an angle α.

Due to the simplicity of actuator disc theory its applications are limited. The standard within the wind industry is to use Blade Element Momentum theory (BEM) for rotor analysis. BEM splits the blade into a number of sections along its length. The forces on each section are then found based on the aerodynamics characteristics of that particular section. The forces on each section are summed to provide the overall performance of the rotor [26, Chapter 3]. This provides a much better representation of the rotor and its blades. As each section of blade is treated in isolation it is assumed that the flow over the blade is two dimensional and therefore the sections do not interact with each other. Additional factors must therefore be added to account for the poorer aerodynamic performance close to the blade tip and root. BEM has become the industry standard for modelling wind turbine rotors. As such there are a number of software tools for analysing turbine rotors with BEM as the core. AeroDyn [34] is one such tool. It is the aerodynamics package used in FAST. As a standalone aerodynamics package AeroDyn allows for more flexibility around its application compared to other BEM based softwares. This makes it more useful to the AWE sector as rotor designs can be very different compared to HAWT.

A key input to AeroDyn and any BEM based tools are the aerodynamic characteristics of the airfoils used on the rotor blades. Therefore values for the lift and drag coefficients and how they change with the wings angle of attack must be known. In the case of rigid airfoils this information is fairly easy to obtain. There is an abundance of wind tunnel data and analysis software freely available for rigid wings. However, this is not the case with soft kites. Due to the complex dynamic behaviour of a kite it is

extremely challenging to describe its aerodynamic characteristics. There is wind tunnel data available for rigid sections of kite profiles [35]. Although this does not take into account the dynamic behaviour of the kites surface, for a steady state analysis these values are adequate.

2.1.3 Tensile Rotary Power Transmission

All AWES must transmit the power that is extracted from the wind down to the ground. As described in Chapter 1 this can either be done mechanically or electrically. Tensile rotary power transmission (TRPT) is a method used to transmit power back down to the ground station mechanically. There are several AWES that use TRPT, these will be introduced in Section 2.2. This power transmission method is able to transfer rotational power from the airborne components down to the ground station. It achieves this by using a series of tensioned lines held apart by rigid components. In its simplest form this consists of two lines held apart by rigid rods along their length, much like a rope ladder. Figure 2.1 shows a diagram of a TRPT system as described in a patent filled by Harburg [1]. So long as there is enough tension on the lines as one end of the system rotates that rotation will continue along the lines to the opposite end of the system. TRPR was first proposed by Harburg [1] in a patent filled in 1991. It has received very little research attention, largely due to its limited application. AWE represents the application where it is perhaps most suited.

The most comprehensive analysis of a TRPT is given by Benhaiem [3, Chapter 22]. Benhaiem analyses the steady state operation of a TRPT used within the rotating reel system, Parotor. Benhaiem also included some initial experimental tests within the analysis. Benhaiem highlights that the geometry of the TRPT plays a decisive role in its ability to transmit power. It is found that the angles at which the lines attach to the rotor on the ground station, the relative sizes of the airborne rotor and the ground station rotor and the length of the power transmission dictate its ability to transmit power. It is concluded that more research is required on TRPT and research on vari-

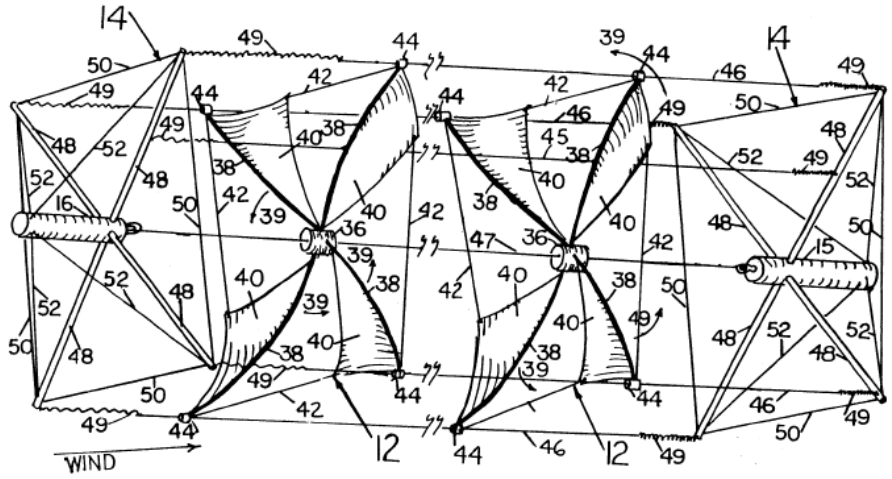

Figure 2.1: Diagram of the coaxial multi-turbine generator as proposed in [1]

ations of the design are needed to better understand TRPT and its application within AWE.

It is noted that as described in [3, Chapter 22] a TRPT system will fail when two adjacent rigid components are out of position by 180°. At this point the lines connecting the rigid components will meet at their midpoint. When this happens the lines will twist and no useful torque can be transmitted by the system.

This Section has given a brief overview of the literature relevant to analysing AWE and in-particular rotary AWES. Much of this is applied within the mathematical model that is described in Chapter 3.

2.2 An Introduction to Rotary Airborne Wind Energy Systems

As previously discussed in Chapter 1 there are a wide variety of AWES designs and concepts at various stages of development. One category is rotary AWES which has received less research attention. Currently the maximum power output that has been

achieved by a rotary system as openly published is 1.4kW. This was achieved by the Daisy Kite in December 2018 [22]. Although rotary AWE devices with larger rated power have been produced there is currently no available evidence showing that they have produced more than 1.4kW. When compared to the power output of other AWE prototypes this is very low especially compared to the three devices highlighted in Chapter 1. However, rotary AWES have a number of distinct advantages that justify their continued research and development. This Section gives a detailed description of rotary AWES, introduces existing rotary AWES prototypes and describes experimental tests that have been undertaken on the Daisy Kite developed by Windswept and Interesting Ltd [21]. This will highlight the advantages that rotary systems have over other AWES designs.

As with all AWES there are three key components to any rotary AWES. These are the ground station, power transmission system and the airborne components that are harvesting the winds power. Many rotary designs also utilise a lifter kite for launching, landing and maintaining tension within the power transmission system. The reason for the need to maintain tension within the power transmission for certain designs will become clear in Section 2.2.2. Figure 2.2 shows a diagram of these key components.

2.2.1 Rotor

The configuration of the airborne wings used within rotary AWES is what distinguishes them from other AWES. Rotary systems utilise multiple wings that are networked together. At its most basic this results in two wings rotating around the same central point. Networking wings together can lead to a number of advantages that include; passive control of wing flight path, increased system redundancy, reduced overall tether drag and improved utilisation of airspace. By networking the wings together the flight path of an individual wing is naturally constrained. Where most AWES require complex control systems to ensure that the desired flight path is followed there are numerous rotary prototypes that require no active control to achieve the desired flight path. Ro-

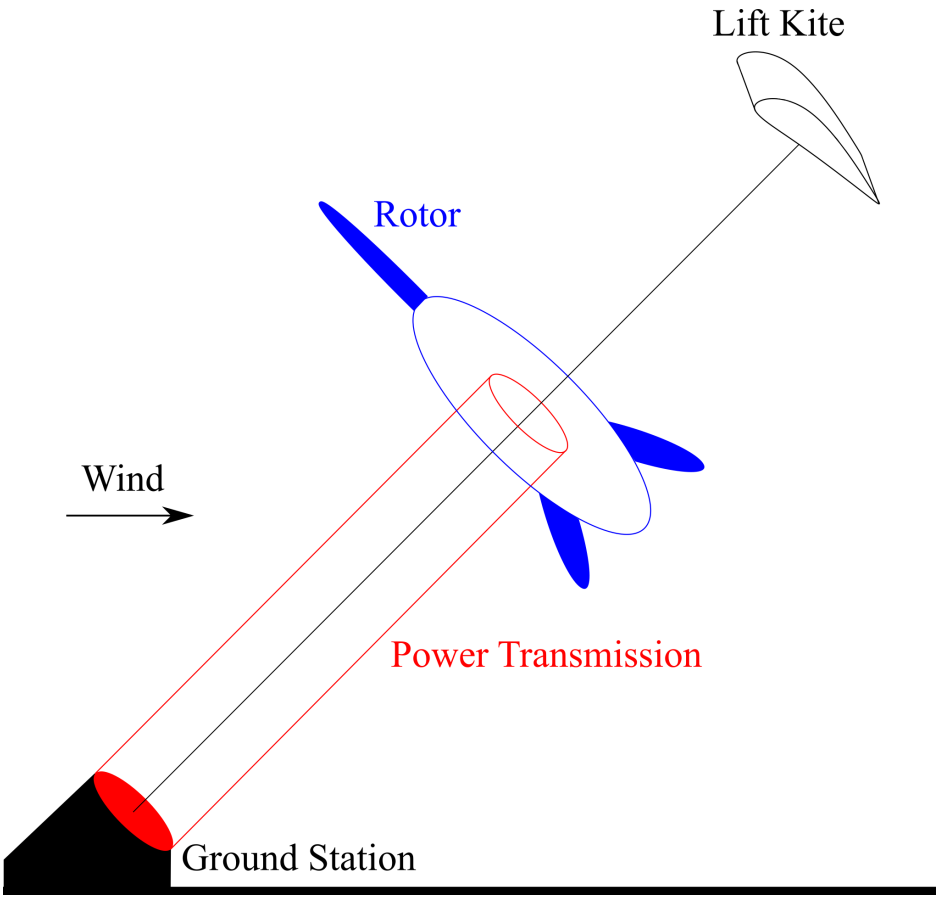

Figure 2.2: Diagram of a Rotary Airborne Wind Energy System

tary systems that are able to achieve this are therefore more inherently stable. It also ensures that there are fewer or in some cases no single points of failure. During field test on the Daisy Kite there were failures in tethers, but these did not cause catastrophic failure. The system is still able to continue operating in a reduced capacity before being retrieved once it is safe to do so. As discussed in Chapter 1 tether drag is a significant source of losses for AWES. There are several rotary AWES where the design is aimed at reducing the systems overall tether drag. For example the KiteX system introduced in Section 2.3.6.

In several designs networked wings or blades form a rotor like that shown in Figure 2.2. The rotor is able to extract power from the wind similar to the rotor of a HAWT. One advantage of AWES that use rotors is that there has already been a large amount

of research into rotor design for HAWT. Although there are differences between the rotor of a HAWT and that of a rotary AWES the methods used to analyse and design HAWT rotors are also applicable to rotary AWES. It is important to note that the rotor of these rotary AWES is able to support at least some of its own weight using aerodynamic lift. To achieve this the rotor relies on autorotation. Autorotation is when an unpowered rotor generates lift as a result of the air passing through the rotor causing the blades to rotate. Autogyros rely on this effect to stay airborne. To achieve autorotation the rotors axis is not parallel with the wind direction. Instead the axis of rotation is pitched downwards towards the ground as can be seen in Figure 2.2. This intentional misalignment of the rotor and the wind direction reduces the potential power that is extracted from the wind for a given rotor size. As described in [26, Chapter 3] a simple analysis shows the power loss is proportional to cubic cosine of the angle between the rotors axis of rotation and the wind direction.

There are many other AWES that use rotors to extract energy from the wind. Several designs of Lighter Than Air and Fly-Gen AWES also use rotors. However, in all these cases when generating power the rotor does not support any of its own weight. Lighter than air AWES use aerostatic lift by means of a shroud filled with a light gas such as Helium. Fly-Gen AWES mount the rotors on a wing that produces sufficient aerodynamic lift. There are designs where multiple Fly-Gen wings are networked together to form a rotary system.

2.2.2 Power Transmission

As described in Chapter 1 AWES must transmit the power down to the ground either mechanically or electrically. Rotary AWES designs that are currently being developed mostly use a mechanical power transmission however there are examples of electrical transmission being used. Sky Windpower introduced in Section 2.3.8 are developing a system with electrical power transmission. To transmit the power electrically a generator is located on the airborne components. As mentioned previously for rotary AWES

that use electrical power transmission wings housing the generators are networked together such that multiple Fly-Gen wings circle about a single central point.

For rotary systems that rely on a mechanical transmission there are three methods. The first and most common within the AWE industry is that of a pumping cycle or 'yo-yo' power generation. Similar to when a single wing is used the tether is reeled in and out on a drum on the ground station. The rotor flies downwind along its axis of rotation and is then pulled back in along the same path. Bladetips Energy introduced in Section 2.3.5 use this pumping cycle generation method. The second method of power transmission uses a tether and two pulleys. The tether is held between the two pulleys one on the ground station the other just underneath the rotor, similar to a belt drive. A series of cogs are used to translate the rotation produced at the rotor by 90° so that the airborne pulley is driven by the rotor. The tether is then pulled over this airborne pulley. As this happens the tether is also pulled over the ground station pulley causing it to spin. The ground station is coupled to a generator for electricity production. Kite Winder introduced in Section 2.3.4 are developing a rotary AWES that transmits the power to ground using this pulley system. The third and final method is tensile rotary power transmission (TRPT). Rotary AWES that use TRPT transfer the rotational motion at the rotor down to the ground station. This is achieved by using a series of tensioned lines held apart by rigid components. With enough tension on the lines the systems will rotate transferring the power from the rotor to the ground station. The Daisy Kite being developed by Windswept and Interesting uses TRPT.

There are advantages and disadvantages for each of the four transmission methods introduced. With electrical power transmission there are advantageous due to the electrical generator being airborne. By running the generator as a motor the launch and landing of the airborne components can be easily controlled. This does however make the airborne components heavier and more fragile. For pumping cycle type transmission, similar to other AWES that use a pumping cycle for transfer power, the airborne components are much more simple. Due to the need to reel the tether back in it is not

possible to have continuous power generation. The reel in phase with a rotary AWES is challenging as the thrust force on the rotor must be minimised. It was suggested by Schutter in [20] this could be used to the systems advantage as for very short pumping cycles the rotor would be allowed to speed up and store kinetic energy during reel in. Schutter showed that this would increase the power extracted over the length of a pumping cycle. For the pulley system the tether drag experienced by the system is reduced as the tethers are not travelling through the air perpendicular to their length. It is envisaged that this method is not suited to larger systems. As the torque from the rotor increases it will become much more difficult to stop the tether from twisting between the two pulleys. An advantage for both the pulley system and TRPT is that the power output is continuous. There are very few AWES currently under development that are able to achieve ground based generation with continuous power out. This is one of the biggest advantages of these rotary AWES over most other Ground-Gen AWE concepts. Perhaps the biggest drawback of TRPT is the potential for very large losses due to tether drag. As highlighted in Section 2.1 the tether drag dominates the losses in an AWES with aerodynamic efficient wings. TRPT relies on a number of tethers passing through the air at high speed which causes a large amount of tether drag.

The power transmission of any AWES drives the design of the overall system. In many cases it will also be the limiting factor in terms of the altitude that can be reached and will play a key role in determining the overall efficiency of the system. It is therefore a crucial component especially in the case of rotary AWES where it has received very little research attention.

2.2.3 Ground Station

The design of the ground station is largely dependent on the power transmission system used. For every AWES the ground station is the main point of contact with the ground. Therefore it must be able to withstand the forces being generated by the airborne components. For systems that use a mechanical power transmission it will

also house the generator. For most AWES the airborne components will be pulled downwind, therefore the ground station must be capable of staying in line with the wind direction. The ground station is also likely to incorporate the launch and landing system. Launching and landing an AWE device can be very complex. There are a number of different methods to achieve it. For those with rotors on the wings vertical or runway take-offs and landings are used. These are relatively simple to be combined into a ground station. In the case where there are no rotors on the wing, which is the case for most mechanical transmission AWES, the ground station can be much more complex. For example EnerKite [36] uses a rotating arm to slowly increase the speed that the wing sees. Once the relative velocity at the wing is large enough such that it is able to support its own weight the wing is slowly released. This was chosen due to research done by Rieck [37]. The opposite process is used for landing. At present most rotary AWES use a lift kite for launching and landing.

2.2.4 Lifter Kite

In most rotary AWES a lift kite is used. For many systems the lift kite is crucial for the launch and landing process. At present all rotary AWES prototypes are small. Therefore a manual launching process is used. The lift kite is thrown into the air by hand much like a traditional kite launch. Once airborne the lift kite then pulls the rest of the system into the air by the tethers. As the systems increase in size a more robust procedure will need to be established. Once the system is airborne the lift kite increases the tension on the tethers. This is advantageous as it allows for greater amounts of power to be transferred down to the ground station. The lift kite can also be used to control the elevation angle of the system. By altering the lift kite used or by adjusting its bridle lines the aerodynamic forces of the lift kite can be adjusted. Although not utilised by any rotary AWES yet it is envisaged that the lift kite can be used to control the rotors power output by altering the systems position relative to the downwind position. Similar to how a small wind turbine is yawed out of the wind to decrease its power output.

2.3 Rotary Airborne Wind Energy System Prototypes

Having introduced the main components of rotary AWES this Section briefly describes the different rotary systems that are being developed.

2.3.1 The Daisy Kite

Windswept and Interesting Ltd. have been developing the Daisy Kite since 2012 [21]. The Daisy Kite uses multiple rotors connected to a single TRPT. The rotors each use three soft kites. The TRPT uses 6 tethers held apart by rings spaced along their length. This results in the tethers making a tube or shaft geometry. Various configurations of the Daisy Kite have undergone many hours of experimental testing. The design with up to three soft kite rotors has been tested as well as a single rotor that uses rigid blades. Figure 2.3 shows a single soft rotor undergoing tests. The latest prototype achieved a power output of 1.4kW in December 2018. This is believed to be the highest power output obtained by any rotary AWES so far. Windswept and Interesting are focused on creating kite networks as described by Read in [3, Chapter 21]. More details on the Daisy Kite are given in Section 2.4.

Figure 2.3: Image of a single rotor Daisy Kite.

2.3.2 Airborne Rotor

Beaupoil has developed a system very similar to the Daisy Kite [19]. Beaupoil's system uses a single rotor with four rigid blades. A TRPT is then used to transfer the power back down to the ground station exactly as with the Daisy Kite. The TRPT system used in Beaupoil's device has a different configuration to that used in the Daisy Kite. Beaupoil's TRPT consists of eight tethers that are held apart by rigid rods. Four of them run straight while the other four run diagonally between the rods. An image of the line set up is shown in Figure 2.4. Beaupoil is currently aiming for a power output of 100W for 100 minutes.

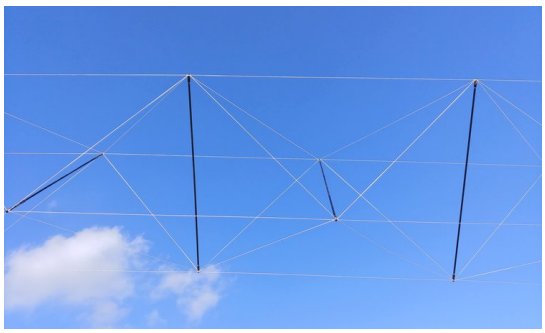

Figure 2.4: Image of the TRPT used within Beaupoil's rotary AWES [2].

2.3.3 Parotor

Benhaiem has developed the Parotor as described in [3, Chapter 22]. Very similar to the Daisy Kite in its design the Parotor uses eight soft kites on a single rotor with a TRPT. In this case the TRPT consists of four tethers equally spaced around the rotors. There are no rigid components other than a rotor at each end of the transmission. The TRPT connects to the ground station on a rotor that is parallel to the ground. Given the elevation angle this means that the tethers in the TRPT change length as the system rotates. This provides a second mode of power generation. A winch is attached to the bottom of each tether. For half of each rotation

Figure 2.5: Image of the Parotor prototype [3].

the tether is being pulled out and therefore generates power. This second mode of generation is similar to how a pumping cycle system works. A small scale prototype has been developed and tested as shown in Figure 2.5. In addition to the four tethers that make up the TRPT the prototype also has several additional suspension lines.

2.3.4 KiweeOne

KiweeOne has been developed by the French based company Kite Winder [4]. KiweeOne is a 100W AWES designed for portable power generation. It uses a two bladed rigid rotor for power extraction and a pulley system as described previously to transmit the power to the ground station. Figure 2.6 shows an image of a KiweeOne prototype undergoing tests. Kite Winder have recently run a crowd funding campaign to help take KiweeOne towards commercial release.

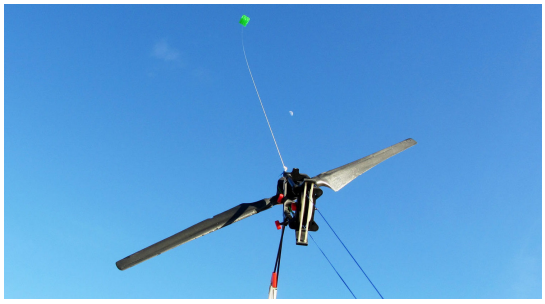

Figure 2.6: Image of a KiweeOne prototype [4].

2.3.5 Bladetips Energy

Bladetips Energy are developing a pumping cycle rotary AWES [5]. It uses a rotor of three rigid blades to pull a tether from a drum at the ground station. Figure 2.7 shows an image of the Bladetips Energy prototype during tests. Founded in 2016 Bladetips Energy are also designing their system for alternative purposes not just electricity production. Their system will be used for telecommunications, surveillance and observation.

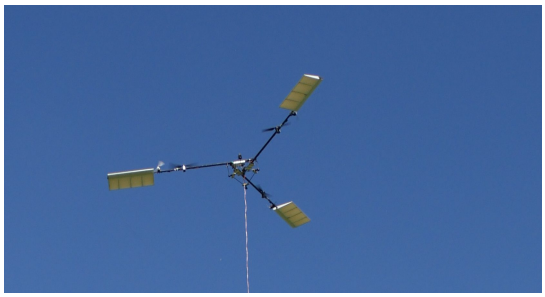

Figure 2.7: Image of the Bladetips Energy prototype [5].

2.3.6 KiteX

KiteX are developing a multi Fly-Gen system [6]. Two rigid wings each with rotors on them fly around the same main tether. Figure 2.8 shows a diagram of the KiteX concept. By using multiple wings the tether drag is greatly reduced. There is a main tether with each wing connected to it by their own secondary tether. The wings use the connection point of the main and secondary tethers as their axis of rotation. This ensures that the main tether can remain relativity still reducing the overall tether drag on the system.

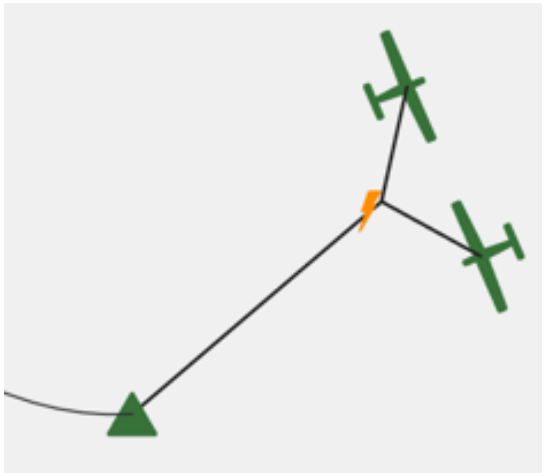

Figure 2.8: Diagram of the KiteX System [6].

2.3.7 Kiteswarms

Kiteswarms are also developing a multi Fly-Gen system [38]. Their system is similar in operation to that of the KiteX system. However, Kiteswarms use more than two wings. Their system uses wings whose secondary tethers are attached along the length of the main tether. The wings are attached in pairs so that the main tether remains relatively still as with KiteX.

2.3.8 Sky WindPower

Sky WindPower use a quad copter for power generation [39]. Figure 2.9 shows an image of Sky WindPower's prototype. The quad copter is flown into the air before it is inclined to the vertical where the four rotors are able to generate lift and power through autorotation. Due to the stationary tether it is envisaged that very high altitudes could be reached as the tether drag will be small compared to many other AWES. Sky WindPower is one of the few companies that are targeting the high altitude jet steams with their device.

Figure 2.9: Image of Sky WindPower's prototype [7].

It can be seen from the eight rotary AWES introduced that there is a large variation between the different concepts. It can also be seen that the Daisy Kite, Beaupoil's airborne rotor and the Parotor are all very similar in design. Windswept and Interesting was founded in 2012 therefore this concept has been around for a number of years. Roberts first proposed the Sky WindPower concept back in the late 1970's. Whereas the use of multiple Fly-Gen wings has only become apparent in the past few years with KiteX and Kiteswarms founded in 2016 and 2017 respectively. This may be due to the recent success that Makani has achieved with their Fly-Gen system and therefore more attention has been given to the application of these systems. Although there are a number different designs none have been developed beyond the small scale prototype stage.

2.4 Experiments on Rotary AWES

Empirical data on rotary AWES has been provided from a series of experimental test conducted using the Daisy Kite at the Windswept and Interesting test site on the Isle of Lewis, Scotland. The Daisy Kite's experimental test campaign is the most comprehensive of any rotary AWES using a tensile rotary power transmission.

2.4.1 Daisy Kite System Configuration

Figure 2.10 shows a diagram of the main components of the Daisy Kite. This Section gives a description of these main components.

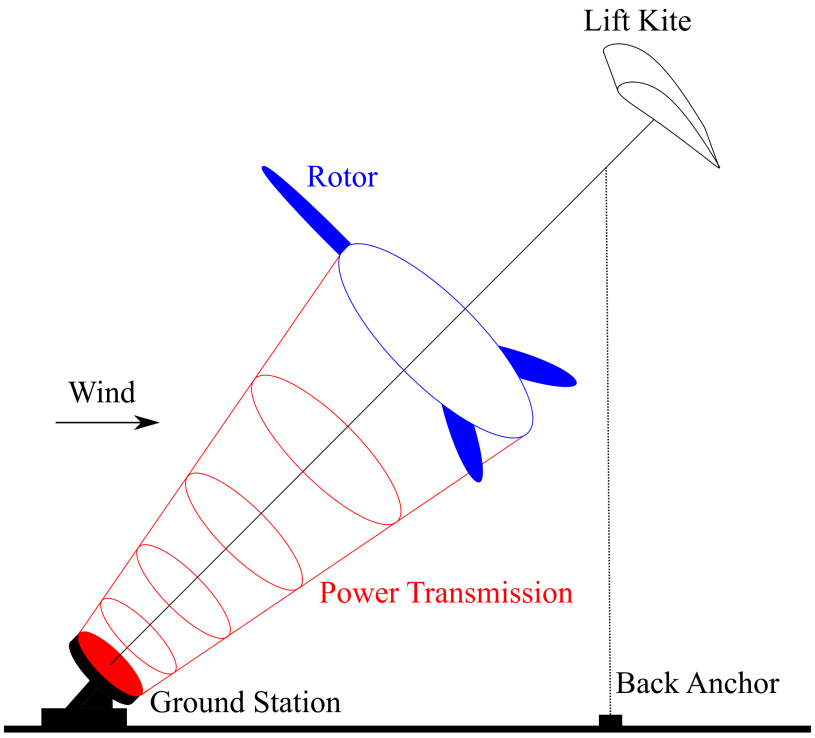

Figure 2.10: Diagram of the Daisy Kite system.

Soft Rotor

The soft rotor set up uses three HQ Symphony Beach III 1.3 kites [40]. These ram air kites have a span of 1.27m and a chord of 0.55m. They are used because of their low cost and ease of availability. The kites are equally spaced around a ring. The ring is made from 4mm carbon fibre tube and has a diameter of 3.04m. The kites are attached to the ring such that the kites outer tips are at a radius of 2.43m. Therefore 0.35m of the kites span are located inside the ring.

Windswept and Interesting have also conducted a series of tests using multiple soft rotors. In these tests additional rotors were added to the system above the initial rotor. Tests on both a 2 and 3 rotor prototype have been carried out. The single rotor Daisy Kite is the focus of this research.

Rigid Rotor

The rigid rotor set up has three foam wings that have NACA 4412 airfoil profiles. These wings have a span of 1m and a chord of 0.2m. Similar to the soft rotor the wings are equally spaced around a 4mm carbon fibre ring that has a diameter of 3.04m. The outer tips of the wings are at a radius of 2.22m therefore 0.28m of the wings span are located inside the ring. The rigid rotor is designed to be as similar as possible to the soft rotor. This allows for a more reliable comparison between the performance of the HQ Kites and the foam wings.

Tests run using the rigid rotor do not use a lift kite. Instead the top of the rotor is attached to a 4.8m mast. This is used as a precaution while the initial tests on the rigid rotor are carried out. By using a fixed mast instead of a lift kite the system becomes inherently stable. It allows the rotor to be fully lifted into the air before it begins to rotate. This avoids the foam wings from striking the ground during launch, operation and landing. Due to the low height of the rotor ground strikes are common with the soft rotor but this does no damage to the HQ Kites. However, ground strikes could

easily cause catastrophic failure of the foam blades. They must therefore be avoided when testing the rigid rotor.

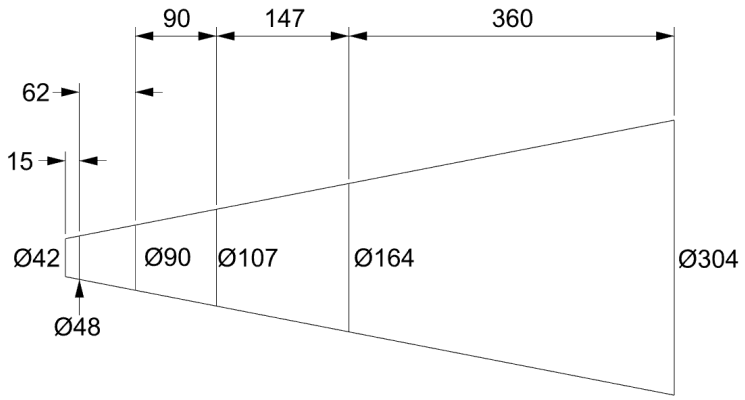

Figure 2.11: Drawing of the Power Transmission used in the Daisy Kite Prototype. All dimensions shown are in centimetres.

Tensile Rotary Power Transmission

The tensile rotary power transmission connects the rotor to the ground station. It consists of six tethers equally spaced around several carbon fibre rings. These rings are placed at various intervals along the tethers and act to keep the 6 tethers apart. A drawing of the power transmission detailing the dimensions of the system is shown in Figure 2.11, its overall length is 6.7m. A cone angle of 22° is used in the system. This is to avoid any abrupt changes in the diameter. As torque is applied the power transmission deforms torsionally. This pulls the tethers in towards the axis of rotation. The carbon fibre rings act to resist this force. When designing the current prototype it was feared that an abrupt change in the diameter would increase the force that the rings must resists beyond their breaking force. Therefore it was decided to slowly decrease the diameter from the rotor down to the ground station.

Ground Station

The tensile rotary power transmission connects to the ground station via a 42cm wheel. This wheel has a Quarq Dzero power meter [41] incorporated into it. The power meter records power and rotational speed. From these the torque can be calculated using $P = Q\omega$ where P is power, Q is torque and ω is rotational speed in rad/s.

The ground station houses a 500W generator. The generator is a 500W ebike motor. The generator connects to the 42cm wheel via a chain drive. The chain drive has a gear ratio of 2.14. The generator is linked to a series of batteries and a Vedder Electronic Stability Controller (VESC) [42]. The VESC is able to set or limit the generator's voltage and current, which controls the systems rotational speed and torque respectively.

The ground station is secured in place using a large screw anchor at its base. The ground station is designed such that it is able to freely rotate around the screw anchor. This ensures that the ground station is pulled into alignment by the rotor. Which in turn ensures that the ground station is aligned with the power transmission.

2.4.2 Windswept and Interesting Testing Set Up

The test site is laid out as shown in Figure 2.12. Due to the test sites proximity to Stornoway airport all components are kept below 30 meters to comply with local airspace regulations. This is achieved by ensuring that the lifter kites tether length is less than 30 meters and that the airborne weight is kept below 2kg. Each testing session must be approved by Stornoway airport air traffic control beforehand. Wind speed and wind direction data is collected using a cup anemometer and wind vane located on the 4 metre met mast. Although the configuration of the Daisy Kite system often changes, which in turn impacts the height at which the rotor operates, the rotors centre is kept close to a height of 4m. This ensures that the wind data is collected at a similar height to the rotor. The wind vane is used to align the system down wind of

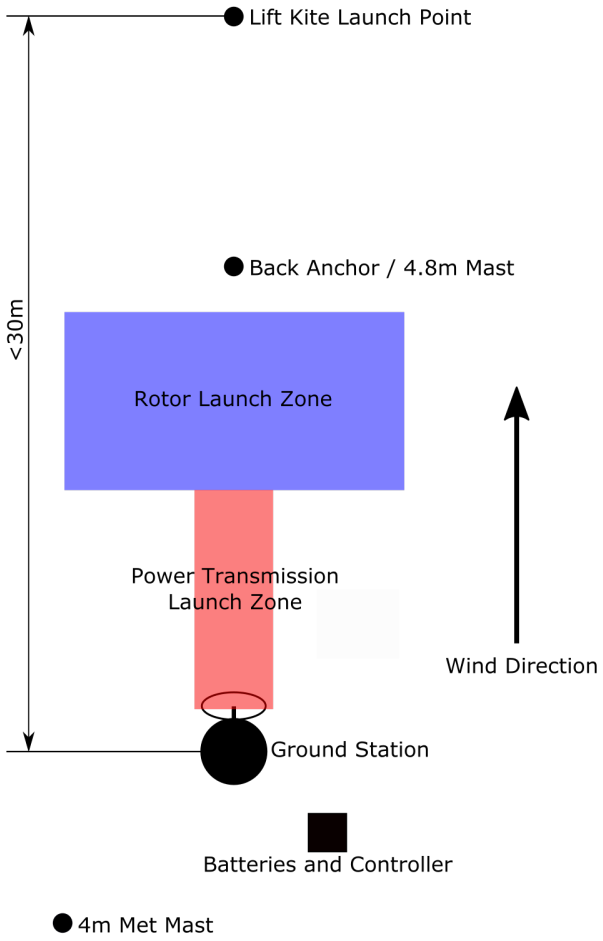

Figure 2.12: Birds eye view of the Windswept and Interesting test site on the Isle of Lewis.

the ground station prior to launching and to monitor any variation in wind direction throughout testing. Both the wind speed and direction are recorded at a rate of 1Hz.

Prior to launching the Daisy Kite is laid out on the ground. The lift kite is then launched with the lift line attached to the back anchor. Once the lift kite is airborne in a stable manner the back anchor is slowly released. The lift kite therefore slowly pulls the rotor and power transmission system into the air. Once airborne the rotor begins to rotate and power is generated. A tether from the lift line to the back anchor remains in place so that the reverse process can be used to land the Daisy Kite.

2.4.3 The Daisy Kite Test Results

The data that has been collected using the Daisy Kite prototype is shown in this Section. All the tests were conducted at the Windswept and Interesting test site. As the Daisy Kite is undergoing continuous development there are constantly small alterations to the system configuration. Many of these design changes are small and will have a negligible impact on the collected data. Where possible the major components have been altered as little as possible to ensure that the data collected in different test runs is comparable.

There have been over 30 days of testing on the Daisy Kite. This has resulted in around 110 hours of test data. Table 2.1 shows a summary of the length of tests that have been carried out on 4 different configurations of the Daisy Kite prototype. Tests have been conducted on both a soft rotor that uses kites and a rigid rotor that uses foam wings.

Rigid or Soft Rotor	Number of Rotors	Length (hours)
Soft	1	49
Soft	2	22
Soft	3	33
Rigid	1	8

Table 2.1: Summary of collected data from the Daisy Kite prototype.

The field tests conducted on the Daisy Kite provide a comprehensive data set for AWES using tensile rotary power transmission. An example of the raw data collected is shown in Figure 2.13.

When analysing the data it was decided to average the values over a set period of time, this is common practise within the wind industry. The data is averaged over both one and five minute periods depending on the analysis being done.

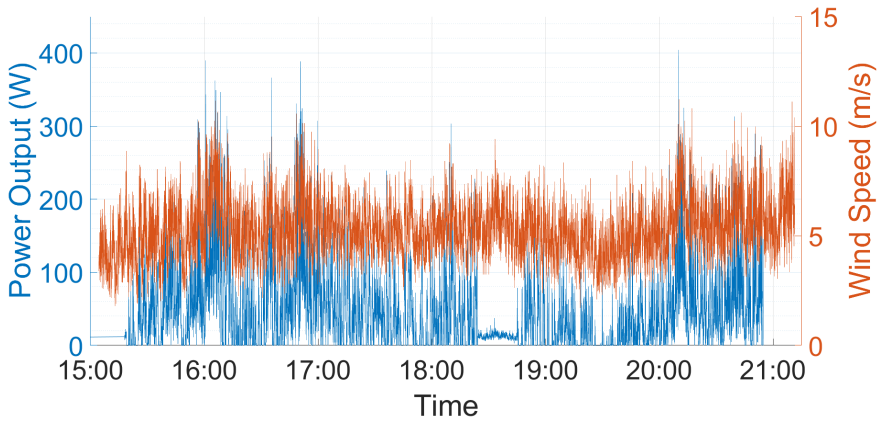

Figure 2.13: Data collected during single soft rotor tests on 22nd August 2018.

One of the tests completed consisted of running a single soft rotor at a number of constant speeds. By running the system at constant speeds more information can be gathered on its operating characteristics. The results of these tests have been used to produce a power coefficient (C_P) against tip speed ratio (λ) plot. This plot is shown in Figure 2.14.

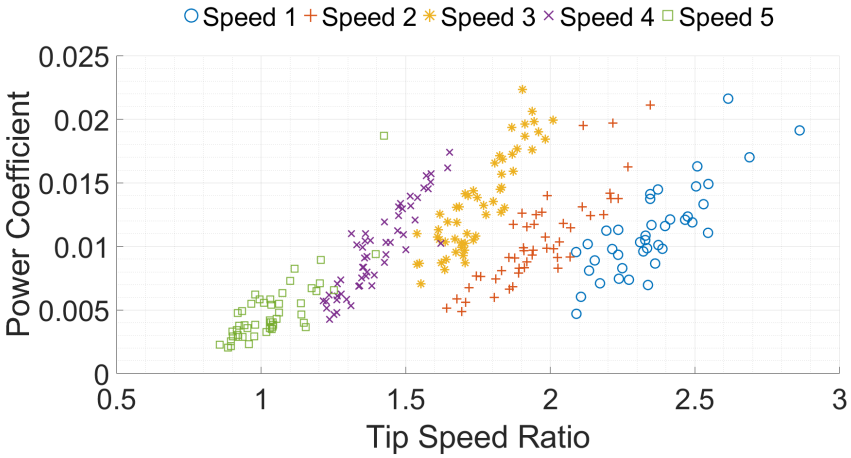

Figure 2.14: Power coefficient against tip speed ratio for single soft rotor constant speed tests.

As can be seen from Figure 2.14 five constant rotational speeds were tested using a single soft rotor. The points shown are one minute averaged values. It can be seen

that the data resembles the shape of a C_P - λ curve for an HAWT, with the power coefficient peaking at 0.02 at a tip speed ratio between 1.5 and 2. For a traditional HAWT power coefficients of 0.3 and above are possible [26]. The power coefficients of the Daisy Kite are therefore very low. This is primarily due to the elevation angle of the system and the use of kites as rotor blades. During the constant speed tests the elevation angle was 50° this theoretically results in a 75% loss in power compared to if the rotors axis was parallel to the wind direction. The kites used on the soft rotor are also of poor aerodynamic design. The poor aerodynamic design also explains the very low tip speed ratio. For an HAWT an optimal tip speed ratio of around 7 would be expected. As can be seen from Figure 2.14 for the Daisy Kite the maximum values of C_P were found at tip speed ratios of just less than 2. Such a low tip speed ratio suggests that a higher solidity rotor would increase the power output. The soft rotor has a solidity of 4.9%. It is suggested that a larger number of blades could be used to increase the power output from a single rotor.

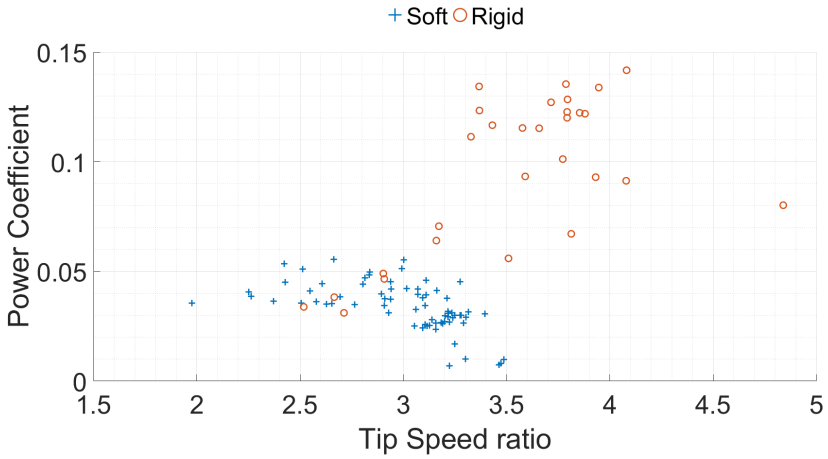

Figure 2.15: Power coefficient against tip speed ratio curve comparing the rigid and soft rotors.

Experiments to compare soft kites to rigid blades were conducted. In these experiments the rotors were not held at constant speed. The main aim of these tests was to experimentally establish an upper limit for what the soft rotor may be able to achieve

with more aerodynamically efficient kites. The C_P - λ plot for these tests is shown in Figure 2.15. The points shown are one minute averaged values. It can be seen from Figure 2.15 that the rigid rotor has a higher power coefficient and tip speed ratio. This is as expected due to the rigid wings being more aerodynamically efficient than the soft kites. It can also be seen that in comparison to Figure 2.14 the power coefficients obtained by the soft rotor during these tests are greater. During the field tests shown in Figure 2.15 the Daisy Kite had an elevation angle of 24°. Therefore the power losses due to the misalignment with the wind direction were much lower. The data collected with the rigid rotor are seen as a upper limit of what can be achieved with the soft kites while maintaining a similar rotor diameter and solidity. The solidity of the rigid rotor is 5.6% similar to that of the soft. As mentioned previously a higher solidity rotor is likely to increase the power output.

Constant speed tests on the rigid rotor were attempted. Unfortunately they were unsuccessful. The rigid rotor is much more responsive to alterations in wind speeds compared to the soft. Although the rigid wings have a better aerodynamic performance their aerodynamic performance is much more sensitive to changes in wind speed. A slight chance in wind speed will cause the rigid rotor to speed up or slow down by a greater magnitude than the soft rotor. This coupled with the time it takes for any change in torque to propagate down the TRPT resulted in the VESC being unable to control the systems rotational speed. The rigid rotors rotational speed oscillated very aggressively. As the rotor slowed the rotational deformation within the TRPT increased, this storing energy within the TRPT. The VESC would then decrease the reaction torque from the generator. The entire system would then rapidly speed up releasing all the stored energy within the TRPT. The VESC would then increase the reaction torque causing the system to slow and the process would repeat. Until the controller can account for how the TRPT changes to variations in torque it will be difficult to accurately control the speed of the rigid rotor. It may also become a problem for the soft rotor if longer transmission systems are used.

This Chapter has introduced rotary AWES. Several different concepts under development show the diverse range of rotary systems. The Daisy Kite developed by Windswept and Interesting has been used to collect over 100 hours of test data, the results from two specific tests have been shown. This data is compared to the mathematical model in Chapter 3.

Chapter 3

Mathematical Modeling of Rotary Kite AWES

This Chapter details the development of a numerical model of rotary AWES, based initially on the Daisy Kite. As highlighted in Section 2.1 rotary AWES have received very little research attention to date. Particularly those that transfer the power to the ground mechanically using TRPT. The development of such systems has been dominated by trial and error using small scale prototypes, which were introduced in Section 2.2. The development of a mathematical model of rotary AWES and specifically a representation of TRPT will aid the development of rotary AWES. It is envisaged that the numerical representation introduced in this Chapter will increase the understanding of, and therefore the speed of development, of rotary AWES.

The modelling process is broken down into a series of individual modules. These modules are dictated by analysing the Daisy Kite system and identifying the main component groups and key modelling parameters. Separating the overall system in this way allows for independent investigations into each module or collection of modules. Modules can be tested, validated and the results analysed in isolation to refine the systems overall design one main component at a time. A block diagram of the various modules and their links with adjacent modules is shown in Figure 3.1. Where T_{lift} is the tension in the lift line, Q_{rotor} and ω_{rotor} the torque and rotational speed

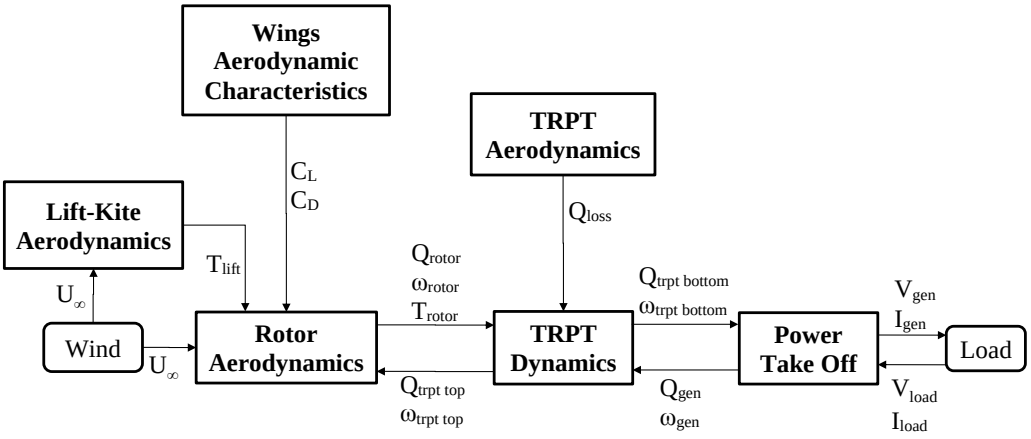

Figure 3.1: Block diagram showing the individual modules that make up the mathematical model of the Daisy Kite system.

produced by the rotor respectively, T_{rotor} the line tension in the TRPT (the product of T_{lift} and the rotors thrust), $Q_{trpt\ top}$ and $\omega_{trpt\ top}$ the torque and rotational speed at the top of the TRPT respectively, Q_{loss} the torque losses within the TRPT due to drag, $Q_{trpt\ bottom}$ and $\omega_{trpt\ bottom}$ the torque and rotational speed at the bottom of the TRPT respectively, Q_{gen} and ω_{gen} the torque and rotational speed of the generator respectively (taking account of any gear ratio used), V_{gen} the generator voltage, I_{gen} the generator current, V_{load} the electrical loads voltage and I_{load} the electrical loads current.

3.1 Rotor Aerodynamics

As can be seen in Figure 3.1 the module on the rotor aerodynamics has a number of inputs from neighbouring modules. The rotor aerodynamics are calculated based on the third party rotor software AeroDynv15 [34]. AeroDynv15 is based on Blade Element Momentum theory, which is widely used within the wind industry and is the standard for analysing rotor aerodynamics [26, Chapter 3]. The adjacent modules provide a number of the required inputs for AeroDynv15.

3.1.1 Wind

For the current model the wind speed is assumed to be uniform and constant. As the model is expanded to investigate larger systems the variation of wind speed in space will become more crucial. Especially as the rotor diameter and operational height increase. Future models will include the impact that a variable wind flow has on the system.

3.1.2 Lift-Kite Aerodynamics

During operation the lift kite increases the line tensions within the system. This increases the ability of the TRPT to transmit torque and is therefore advantageous. With the current steady state model the lift produced by the lift kite is found from the basic aerodynamic equations for lift and drag shown in (3.1a) and (3.1b) where L is the lift force , D is the drag force and S the kite area .

$$L = \frac{1}{2}\rho V^2 S C_L \tag{3.1a}$$

$$D = \frac{1}{2}\rho V^2 S C_D \tag{3.1b}$$

The lift and drag are then resolved in line with the tether to give the line tension in the lifting line and therefore the lift kites contribution to tension. The lift kite used in the Daisy Kite is a single skin Peter Lynn lift kite [43]. This is a bespoke kite and therefore its aerodynamic characteristics have been estimated based on available literature [9]. An example analysis of the lift kites contribution to tension is shown in Table 3.1.

C_L	1
C_D	0.2
Wind Speed	7 m/s
Kite area	3.2 m^2
System elevation angle	50°
Contribution to line tension	155N

Table 3.1: Example analysis for the lift kites contribution to the systems line tension.

3.1.3 Wing Aerodynamic Characteristics

A key input into the model are the aerodynamic properties of the wings used within the rotor. The most important factors being the lift and drag coefficients and how these vary with the wings angle of attack. It has not been possible to obtain these values for the HQ Symphony Beach III 1.3 kites that are used on the soft rotor. The properties have therefore been based on the available ram-air kite literature. For key angles of attack from 0° to 30° the values measured by Seidel [35] during wind tunnel tests on a ClarkY-M15 are used. Outside of this range these values are extrapolated such that the coefficients vary with the angle of attack as defined in [44]. Figure 3.2 shows the ratio of C_L to C_D and how this varies with the angle of attack of the wing.

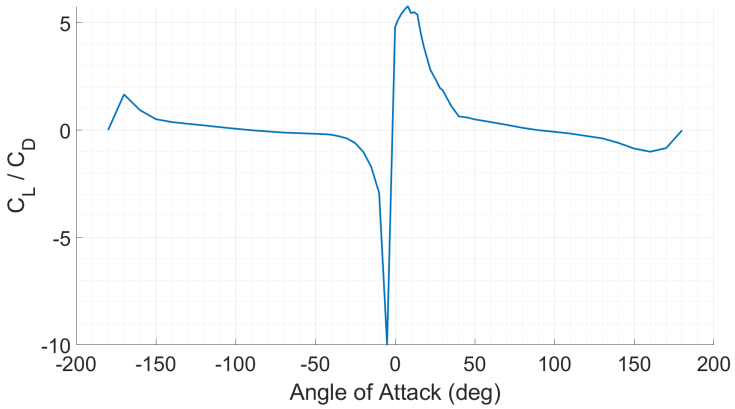

Figure 3.2: Aerodynamic characteristics used to model the kites properties.

The foam wings used on the rigid rotor are based on the NACA 4412 airfoil profile. The aerodynamic characteristics for the rigid wings are based on the wind tunnel data values measured by Ostowari [45].

As previously mentioned the rotor aerodynamics module is based on the software package AeroDyn v15. Along with the input from the *Wind*, *Lift-Kite Aerodynamics* and *Wing Aerodynamic Characteristics* there are several other input parameters required. One of these is the wing geometry. In the case for the soft rotor the kite geometry has been approximated as shown in Figure 3.3. For the rigid blades the chord length is uniform along the span at 0.2m.

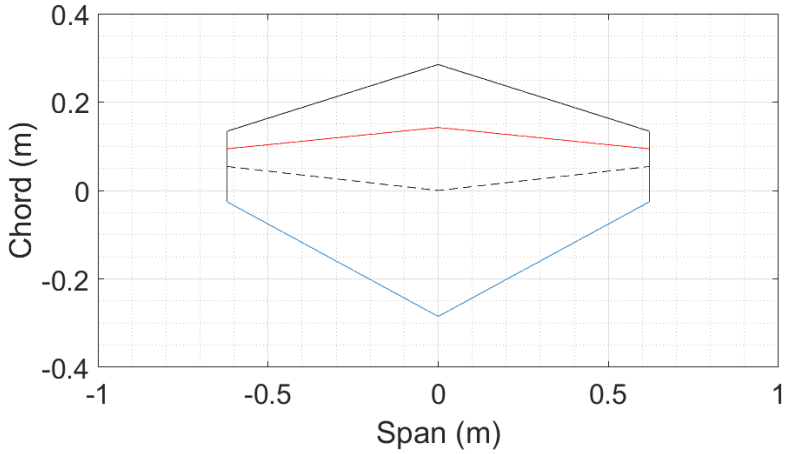

Figure 3.3: Geometry of the kite used as input to AeroDynv15.

The AeroDyn v15 input files used can be found in Appendix A, these show the full range of input parameters. Over the course of the simulations three input parameters have been varied largely driven by the data collected during the experimental tests. The wind speed has been varied from 2m/s to 12m/s and the rotational speed from 10rpm to 150rpm. This ensures that simulations have been run for all the situations experienced within the experimental test campaign. The third input to be altered is the *Shaft Tilt* which corresponds to the elevation angle of the Daisy Kite system. As previously stated when running the fixed mast tests the elevation angle was constant at 24.2°. When using the lifter kite the elevation angle can very greatly depending on the wind conditions, for the series of constant speed tests that were run it was measured to be around 50°. The *Shaft Tilt* has therefore been set at both 24.2° and 50° for simulations.

3.2 Tensile Rotary Power Transmission

As introduced previously the TRPT within the Daisy Kite uses several carbon epoxy rings to separate the 6 tethers. Of key interest is the maximum value of torque that this configuration can transfer before collapse and what the losses are from the rotor to the ground station. These two factors are investigated by considering the steady state operation and the aerodynamics of the TRPT configuration used in the Daisy Kite.

3.2.1 Static Analysis

The steady state operation of the Daisy Kites power transmission is analysed by assuming a static equilibrium in one section of the TRPT. This directly expands on the work done by Tulloch [46]. A diagram of a single section and single tether is shown in Figure 3.4. The forces experienced at the tether connection point are as follows; F_x parallel with the axis of rotation of the TRPT, F_t tangential to the ring and F_r towards the axis of rotation. These correspond to the TRPT tension, torque and compression respectively. L is the length of the tether, R the radius of the ring, c the length of the chord line that joins the connection point at the top and bottom of the tether superimposed on the bottom ring, δ the rotational deformation between the two rings and β the angle that the tether makes relative to its original position. For this analysis the two rings are the same diameter.

The contribution to torque on the bottom ring from a single tether is determined by (3.2).

$$Q = R\ F_t \tag{3.2}$$

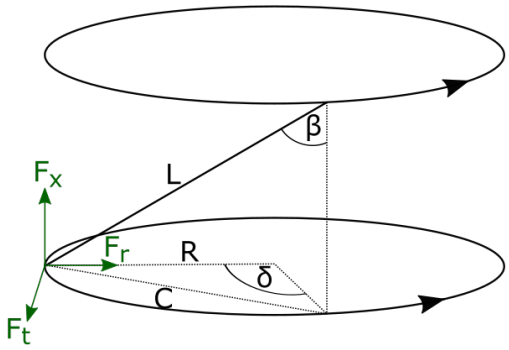

Figure 3.4: Diagram showing a single tether within the Daisy Kites tensile rotary power transmission.

From analysing the diagram shown in Figure 3.4, (3.3a), (3.3b) and (3.3c) can be formed. It is noted that (3.3c) uses the standard equation for chord length.

$$F_t = F_c \; cos\left(\frac{\delta}{2}\right) \tag{3.3a}$$

$$F_c = F_x \; tan(\beta) \tag{3.3b}$$

$$c = 2 \; R \; sin\left(\frac{\delta}{2}\right) = L \; sin(\beta) \tag{3.3c}$$

By substituting (3.3a) and (3.3b) into (3.2), (3.4) is found.

$$Q = R \; F_x \; tan(\beta) \; cos\left(\frac{\delta}{2}\right) \tag{3.4}$$

By rearranging (3.3c), (3.5) is found.

$$sin(\beta) = \frac{2R}{L} \; sin\left(\frac{\delta}{2}\right) \tag{3.5}$$

$$tan(\beta) = \frac{sin(\beta)}{cos(\beta)} = \frac{sin(\beta)}{\sqrt{1 \ - \ sin^2(\beta)}} \tag{3.6}$$

Substituting (3.5) and the trigonometry relationship shown in (3.4) into (3.4), (3.7) is found.

$$Q = R \ F_x \ \frac{\frac{2R}{L} \ sin\left(\frac{\delta}{2}\right) \ cos\left(\frac{\delta}{2}\right)}{\sqrt{1 \ - \ \left(\frac{2R}{L} \ sin\left(\frac{\delta}{2}\right)\right)^2}} \tag{3.7}$$

(3.7) can be rearranged to form (3.8)

$$Q = R \ F_x \ \frac{sin\left(\frac{\delta}{2}\right) \ cos\left(\frac{\delta}{2}\right)}{\sqrt{\frac{1}{2}\left(\frac{L^2}{2R^2} \ - \ 1 \ + \ 1 \ - \ 2sin^2\left(\frac{\delta}{2}\right)\right)}} \tag{3.8}$$

$$sin\left(\frac{\delta}{2}\right) \ cos\left(\frac{\delta}{2}\right) \ = \frac{sin(\delta)}{2} \tag{3.9}$$

$$cos(\delta) \ = \ 1 \ - \ 2sin^2\left(\frac{\delta}{2}\right) \tag{3.10}$$

By substituting the trigonometry relationships shown in (3.9) and (3.10) into (3.8) the expression for torque shown in (3.11) is found.

$$Q = \frac{R \ F_x}{\sqrt{2}} \ \frac{sin(\delta)}{\sqrt{\frac{L^2}{2R^2} + cos(\delta) - 1}} \tag{3.11}$$

It is therefore shown that the ability of the TRPT to transmit torque is dependant on three factors: the radius of the rings, the length of the tethers and the systems tension. Although this has been known previously the relationships between them is confirmed analytically with (3.11).

For a given operational point the torsional deformation of the TRPT can be found using (3.11). In order to find the maximum torque that can be transmitted (3.11) is differentiated with respect to the torsional deformation δ to give the torsional stiffness (K) as shown in (3.12).

$$K = \frac{R\ F_x}{\sqrt{2}} \left(\frac{cos(\delta)}{\sqrt{\frac{L^2}{2R^2} + cos(\delta) - 1}} + \frac{sin^2(\delta)}{2\left(\frac{L^2}{2R^2} + cos(\delta) - 1\right)^{\frac{3}{2}}} \right) \tag{3.12}$$

Figure 3.5 shows the torque and torsional stiffness against the torsional deformation of a single TRPT section. In this case the tether length is 1m, ring radius 0.4 and the overall tension in the TRPT is 544N. The overall tension is found by combining the thrust from the rotor with the line tension produced by the lift kite.

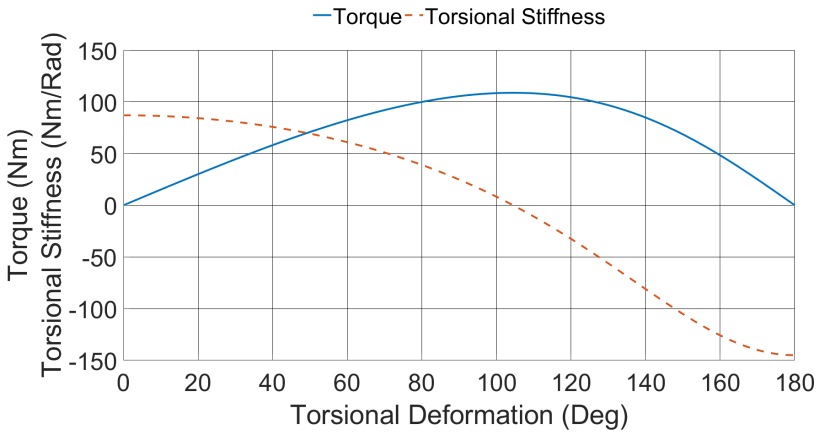

Figure 3.5: Variation of torque and stiffness in the relation to the torsional deformation within a tensile rotary power transmission.

It can be seen from Figure 3.5 that in this case the torque peaks at a value of just over 100Nm at a torsional deformation of a little over 100°, where the torsional stiffness is 0. Above this value of torque the TRPT will over twist and the tethers will cross therefore the TRPT will no longer transmit torque. Previously it was thought that the TRPT will not fail until a torsional deformation of 180° has been reached [3, Chapter 22]. The analysis shows that this is not the case and that the system will fail at smaller values of torsional deformation.

Knowing the maximum torque and the torsional deformation at which this occurs is helpful both in terms of system design and operational control. By setting the torsional stiffness as shown in (3.12) to zero the torsional deformation at which the maximum value of torque occurs, referred to as δ_{max}, can be found. The result is shown by (3.13) were φ is given by (3.14).

$$\delta_{max} = cos^{-1}\left(1 - \frac{\varphi^2}{2} + \frac{\varphi}{2}\sqrt{\varphi^2 - 4}\right) \tag{3.13}$$

$$\varphi = \frac{L}{R} \tag{3.14}$$

By analysing (3.13) it can be stated that the maximum torsional deformation is dictated only by the ratio of the tether length to the ring radius. Therefore there is no need to know the specific operating condition to determine the maximum torsional deformation. This is advantageous when it comes to operational control of the system. For a given section of the TRPT it is possible to set a limit on the maximum torsional deformation according to the geometry and thereby ensuring that the TRPT never exceeds its maximum torque. Figure 3.6 shows how the value of torsional deformation at which the maximum torque occurs (δ_{max}) varies with the ratio of tether length to TRPT radius (φ).

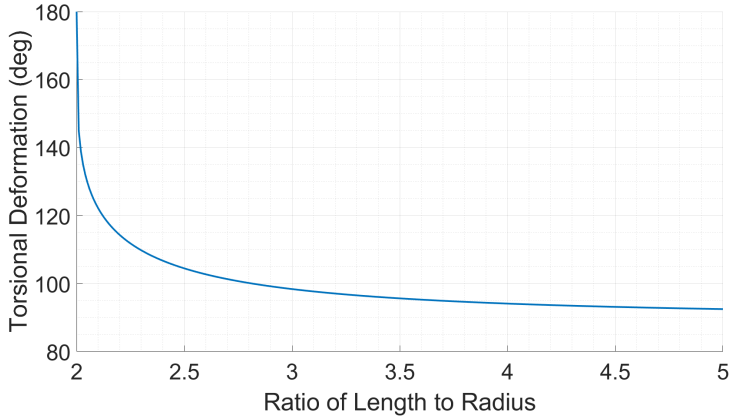

Figure 3.6: Torsional deformation at which the maximum torque can be transmitted for tensile rotary power transmission.

The maximum value of torque can be found by substituting (3.13) into (3.11). The result of this is shown in Figure 3.7. Figure 3.7 shows the maximum value of torque plotted against the ratio of tether length to TRPT radius (φ).

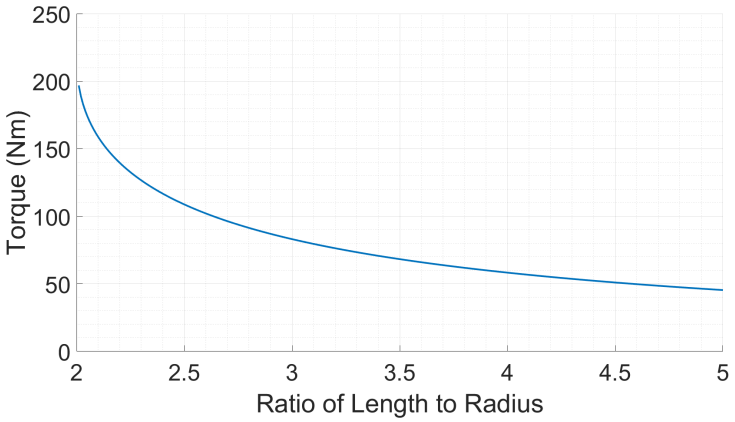

Figure 3.7: The maximum torque that can be transmitted for tensile rotary power transmission.

By analysing (3.11) it can be stated that the maximum value of torque is directly proportional to the overall tension on the TRPT. Therefore by increasing the tension the maximum torque will also increase by the same ratio.

It is worth noting that this analysis can only be used to predict the maximum torque

when the ratio of the tether length to TRPT radius is greater than 2. If the tether length is less than the diameter of the TRPT then it is not geometrically possible for the TRPT to over twist to the point at which the tethers cross. In this case the maximum torque is dictated by either the strength of the tethers or the strength of the rings within the TRPT.

3.2.2 Tether Aerodynamics

Within the TRPT there will be power losses. As with many AWES these losses are dominated by the aerodynamic drag on the tethers [3, Chapter 2]. Therefore it is only the tether drag that has been considered in this case. The tether drag can be found using (3.15). Where C_{Dt} is the tethers drag coefficient of 1, d the tether diameter, l_t the tether length and V_t the apparent wind speed seen by the tether.

$$D_t = \frac{1}{2}\, C_{Dt}\, \rho\, d\, l_t\, V_t^2 \tag{3.15}$$

The losses within the TRPT are considered as torque losses therefore by multiplying the tether drag force D_t by the TRPT radius a loss in torque can be found. The TRPT used within the Daisy Kite has a cone shape as shown in Figure 2.11 therefore the radius is constantly changing. The mid point of each section is used to find the tether drag and contribution to torque loss of each section. Using data collected on the 23$^{\text{rd}}$ August 2018 when an average power output of 54.7W was achieved at an average wind speed of 4.1 m/s. The torque losses are found to be 1.57Nm. This corresponds to a TRPT efficiency of 83.9%. The TRPT efficiency varies greatly depending on the operating conditions. However on the whole the current TRPT efficiency is very low especially considering that the overall length of the TRPT is only 6.7m. It is also noted that the wings bridle lines have not been accounted for here therefore the actual losses are likely to be greater than currently calculated.

3.3 Rotary AWES Model

Combining all the modules excluding the *Power Take Off* and *Load* modules allows the Daisy Kites mechanical power output to be predicted. As mentioned in Section 2.2 the power meter on the Daisy Kite prototype is located at the bottom of the TRPT. Therefore for comparison to the experimental data there is no need to include the final two modules of the mathematical model. Figure 3.8 shows the experimental results compared to the models prediction. The experimental data points shown are 5 minute averaged values.

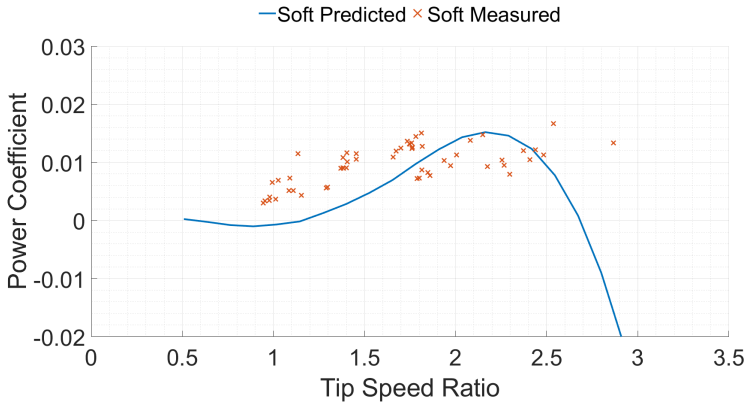

Figure 3.8: Comparison between the mathematical model and the single soft rotor constant speed tests.

From Figure 3.8 it can be seen that the predicted power output from the mathematical representation is comparable to the experimental data collected using the soft rotor during the constant rotational speed tests. The power coefficients in this case are very low compared to those achieved by a traditional HAWT. The elevation angle of 50° during the tests and the poor aerodynamic performance of the soft kites are the main reasons for this. Figure 3.9 shows the comparison between the model and the experimental data for both the soft and rigid rotor. Again, the experimental data points shown are 5 minute averaged values.

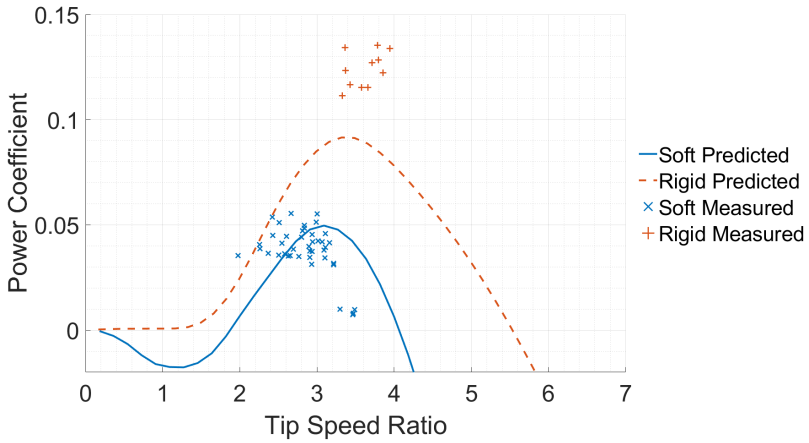

Figure 3.9: Comparison between the mathematical model and single rotor tests.

It can be seen from Figure 3.9 that the model of the soft rotor is closer to the experimental data compared to the rigid rotor. This is not as expected, prior to comparing the results it was assumed that the rigid rotor results would match more closely than the soft rotor. There is more literature available on the performance of rigid airfoils than that available for kites. The aerodynamic characteristics used for the rigid airfoil are for the specific airfoil profile used. Whereas, for the kites the aerodynamic characteristics used are for a similar airfoil profile but not the profile on the kites. Therefore it was initially assumed that the rigid rotor model would match the empirical data more closely than the soft rotor. Figure 3.9 shows that this is not the case. Comparing Figures 3.8 and 3.9 it can be seen that the power coefficients are greater in Figure 3.9. This is due to the data for Figure 3.9 being collected using a fixed mast instead of a lifter. Therefore the elevation angle is lower leading to higher power outputs.

This Chapter has introduced a mathematical model of rotary AWES based on the Daisy Kite. It has been shown through comparison to experimental data that the output from the current mathematical model reliably predicts the Daisy Kites power output.

Chapter 4

Conclusions and Future Works

This Chapter concludes this report and gives a summary of the 2nd year of this PhD research project. The aim of this research is to improve the understanding of rotary AWES and aid their development. This has been done through the development of a mathematical model and a small scale prototype. The small scale prototype has been developed in collaboration with Windswept and Interesting Ltd. A further iteration of their AWES, the Daisy Kite, was produced with this research as its main driver. Section 2.2 detailed the prototype iteration. The issues highlighted with the data collection process at the end of the 1st year of this research have been resolved with the current prototype. A series of tests were run on the improved prototype at the Windswept and Interesting test site on the Isle of Lewis. The results from these tests were shown in Section 2.2.

The main aim for collecting data is for comparison to the mathematical model. This comparison has been shown in Chapter 3. Chapter 3 also detailed the progress that has been made on developing a mathematical model. The aerodynamic aspects of the model rely on AeroDyn, a third party rotor aerodynamics software package based on BEM. AeroDyn was chosen over other available software packages due to it being a standalone aerodynamics package. It provides more flexibility compared to alternatives. Previously a BEM model had been developed but it was found that the results from AeroDyn were much more accurate.

The tensile rotary power transmission model makes up a crucial component of this research. As this method of power transmission is not used anywhere else there is very little analysis of it. By producing a mathematical representation of the TRPT the knowledge around it will drastically improve. It will also allow investigations into the limitations in terms of scale, which will in turn provide an analysis of the scalability of rotary AWES using this power transmission. The analysis shown in Chapter 3 is a simple steady state balance of the forces within the TRPT. This has provided details around the geometrical design for a desired torque given a set tension. Using this analysis it is possible to refine the design of a TRPT. However, the dynamic response of the power transmission is key to the systems performance and any control system that is used. This is highlighted in Section 2.2 where experimental tests on rigid rotors were unsuccessful. It was not possible to maintain a constant rotational speed for a rigid rotor. This was largely down to the control system not accounting for the dynamic behaviour of the TRPT properly. If the operation of TRPT is to be improved a mathematical representation of the dynamic response is needed.

The comparison of the experimental data to the model in Chapter 3 summaries the progress that has been made in the last 12 months. The model now reasonably well represents the steady state performance of the Daisy Kite AWES. This has been down to both the improvements seen in experimental set up and the data collection during tests. The ability to reliably run constant speed tests on the soft rotor provided multiple operational points to compare with the model. Equally the inclusion of the aerodynamics package AeroDyn to the model provided a much improved representation of the Daisy Kites rotor performance. With a reliable representation of the steady state performance moving towards a dynamic model is now the focus of this research.

4.1 Work Plan for Year 3

From the progress made so far a number of key areas of development have been highlighted. The main one being a dynamic representation of the TRPT. Therefore the next few months shall be spent developing the mathematical model to incorporate this. Once this has been achieved the model will be used to investigate rotary AWES. This will have three aspects as its focus:

- The first to explore the design space with the aim of improving the design of the Daisy Kite. To achieve this similar rotary AWES will be investigated. Sensitivity analysis will be done on various inputs to the model including aerodynamic properties and the systems geometry. This will help to inform another design iteration to increase the performance of the Daisy Kite.

- Secondly the model will be used to assess the scalability of rotary AWES. The potential target market for rotary AWES will depend on their suitability for larger scale systems. No rotary AWES has achieved a power output of greater than 1.4kW while there are several other AWES being manufactured that are 100kW+. The feasibility of a rotary AWES at this scale will be analysed.

- Having used the model to investigate the systems design and scalability it will be used to design an operational strategy for rotary AWES. This will focus on ensuring stable operation of the whole system. With an operational strategy designed an investigation into potential control methods to follow this strategy will be done. If rotary AWES are to increase in size autonomous control of the devices must be incorporated. This includes the launching and landing of the systems.

Figure 4.1 shows a Gantt Chart of the proposed time line to allow the work detailed above to be carried out in the next 12 months.

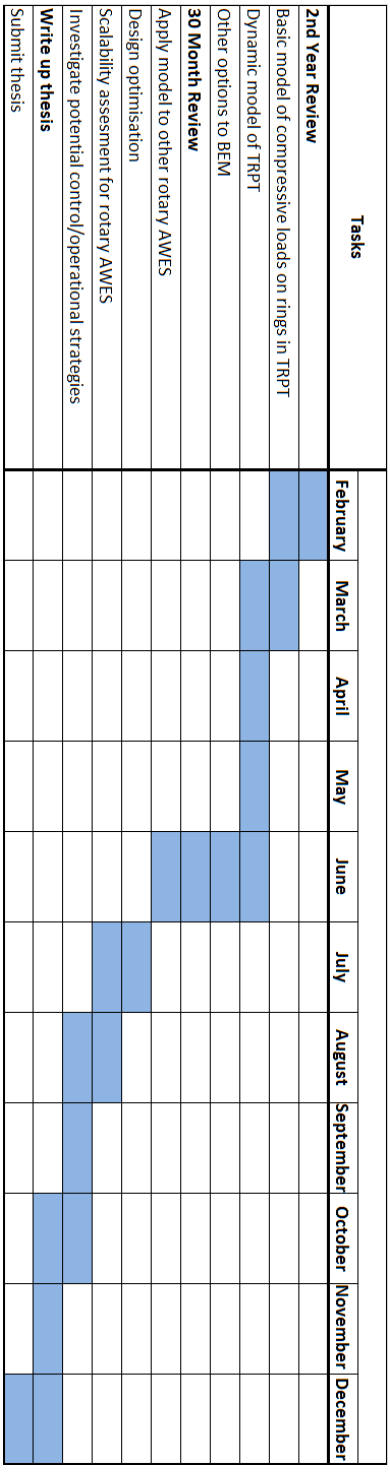

Figure 4.1: Gantt Chart for 3rd Year of PhD.

Bibliography

[1] R. W. Harburg, "Coaxial multi-turbine generator," 20 1991, uS Patent 5,040,948.

[2] C. Beaupoil. Some airborne wind energy. [Online]. Available: https://www.someawe.org/

[3] R. Schmehl, *Airborne Wind Energy - Advances in Technology Development and Research*, 2nd ed. Springerlink, in press 2018.

[4] Kite winder. [Online]. Available: https://kitewinder.fr/

[5] Bladetips energy. [Online]. Available: http://bladetipsenergy.com/en/home/

[6] Kitex. [Online]. Available: http://kitex.tech/prototypes/

[7] Sky windpower. [Online]. Available: https://www.skywindpower.com/index.htm?_p=Y

[8] R. E. P. N. for the 21st Century, *Renewables 2018 Global Status Report*. Paris, France: Paris: REN21 Secretariat, 2018.

[9] U. Ahrens, M. Diehl, and R. Schmehl, *Airborne wind energy*, 1st ed., ser. Green energy and technology. Springerlink, 2013.

[10] C. L. Archer and K. Caldeira, "Global assessment of high-altitude wind power," *Energies*, vol. 2, no. 2, pp. 307–319, 2009. [Online]. Available: http://www.mdpi.com/1996-1073/2/2/307

[11] P. Bechtle, M. Schelbergen, R. Schmehl, U. Zillmann, and S. Watson, "Airborne wind energy resource analysis," *arXiv.org*, 2018. [Online]. Available: http://search.proquest.com/docview/2093221246/

[12] L. Fagiano and M. Milanese, "Airborne wind energy: An overview," in *2012 American Control Conference (ACC)*, June 2012, pp. 3132–3143.

[13] A. Cherubini, A. Papini, R. Vertechy, and M. Fontana, "Airborne wind energy systems: A review of the technologies," *Renewable and Sustainable Energy Reviews*, vol. 51, no. Supplement C, pp. 1461 – 1476, 2015. [Online]. Available: http://www.sciencedirect.com/science/article/pii/S1364032115007005

[14] R. Schmehl, "Worldmap awe activities 2017," 2017, Reseach Gate Project: AWESCO - Airborne Wind Energy System Modelling, Control and Optimisation. [Online]. Available: https://www.researchgate.net/publication/320297363_Worldmap_AWE_activities_2017

[15] Makani. (2017) Makani Kites: airborne wind energy. [Online]. Available: https://www.x.company/makani/

[16] F. Felker. (2019) Makani takes to the ocean with Shell. [Online]. Available: https://blog.x.company/makani-takes-to-the-ocean-with-shell-5aa74551917a

[17] KPS. (2019) Kite Power Systems. [Online]. Available: http://www.kps.energy/

[18] A. Power. (2017) The Energy of Tomorrow. [Online]. Available: https://www.ampyxpower.com/

[19] C. Beaupoil, "Rotary airborne wind energy systems with ground based power generation: Overview and practical experiences," in *Book of Abstracts of the Airborne Wind Energy Conference 2017*, M. Diehl, R. Leuthold, and R. Schmehl, Eds. Freiburg, Germany: Albert Ludwigs University of Freiburg and Delft University of Technology, 2017, p. 133. [Online]. Available: http://resolver.tudelft.nl/uuid:3ea60c17-e582-4b76-8992-faf92b6f611d

[20] J. D. Schutter, R. Leuthold, and M. Diehl, "Optimal control of a rigid-wing rotary kite system for airborne wind energy," in *2018 European Control Conference (ECC)*, June 2018, pp. 1734–1739.

[21] R. Read. (2017) Windswept and Interesting - Kite Power No Tower. [Online]. Available: https://www.windswept-and-interesting.co.uk/

[22] ——. (2017) Rod Read's Youtube Channel. [Online]. Available: https://www.youtube.com/user/roddyread

[23] D. Yinke, *Ancient Chinese Inventions*. Cambridge, UK: Cambridge University Press, 2011.

[24] M. Loyd, "Crosswind kite power," *Journal of Energy*, vol. 4, no. 3, pp. 106–111, 1980.

[25] I. Argatov, P. Rautakorpi, and R. Silvennoinen, "Estimation of the mechanical energy output of the kite wind generator," *Renewable Energy*, vol. 34, no. 6, pp. 1525–1532, 2009.

[26] T. Burton, D. Sharpe, N. Jenkins, and E. Bossanyi, *Wind Energy Handbook*, 1st ed. Wiley, 2001.

[27] M. De Lellis, R. Reginatto, R. Saraiva, and A. Trofino, "The betz limit applied to airborne wind energy," *Renewable Energy*, vol. 127, pp. 32–40, 2018.

[28] P. Jamieson, *Innovation in Wind Turbine Design*, 2nd ed., 12 2018.

[29] A. Energies. Clean energy. [Online]. Available: http://www.altaeros.com/energy.html

[30] UK Government, "Contracts for difference second allocation round results," sep 2017. [Online]. Available: https://assets.publishing.service.gov.uk/government/uploads/system/uploads/attachment_data/file/643560/CFD_allocation_round_2_outcome_FINAL.pdf

[31] ofgem. Electricity prices: Day-ahead baseload contracts monthly average (gb). [Online]. Available: https://www.ofgem.gov.uk/data-portal/electricity-prices-day-ahead-baseload-contracts-monthly-average-gb

[32] S. Mann, "An introduction to airborne wind technology and cost reduction trends," 2019.

[33] KPS. (2017) http://www.kps.energy/kite-power-systems-moves-to-new-glasgow-offices/. [Online]. Available: http://www.kps.energy/kite-power-systems-moves-to-new-glasgow-offices/

[34] NREL. (2019) AeroDyn. [Online]. Available: https://nwtc.nrel.gov/AeroDyn

[35] M. Ghoreyshi, K. Bergeron, J. Seidel, A. Jirasek, A. J. Lofthouse, and R. M. Cummings, "Prediction of aerodynamic characteristics of ram-air parachutes," *Journal of Aircraft*, vol. 53, no. 6, 2016.

[36] EnerKite. Enerkite airborne wind energy. [Online]. Available: http://www.enerkite.de/en/

[37] B. Rieck, M. Ranneberg, A. Candade, A. Bormann, and S. Skutnik, "Comparison of launching and landing approaches," in *Book of Abstracts of the Airborne Wind Energy Conference 2017*, M. Diehl, R. Leuthold, and R. Schmehl, Eds. Freiburg, Germany: Albert Ludwigs University of Freiburg and Delft University of Technology, 2017, p. 123. [Online]. Available: http://resolver.tudelft.nl/uuid:746d1263-9685-452a-b26b-d26b6a138c65

[38] Kiteswarms. [Online]. Available: https://kiteswarms.com/

[39] B. W. Roberts, D. H. Shepard, K. Caldeira, M. E. Cannon, D. G. Eccles, A. J. Grenier, and J. F. Freidin, "Harnessing high-altitude wind power," *IEEE Transactions on Energy Conversion*, vol. 22, no. 1, pp. 136–144, March 2007.

[40] H. Kites. (2019) SYMPHONY BEACH III 1.3 RNBOW. [Online]. Available: http://hqkitesusa.com/proddetail.asp?prod=11768050

[41] Quarq power meters. [Online]. Available: https://www.quarq.com/dzero/#sm.0001mr3ju1pktd57qde19rnfjf0fp

[42] B. Vedder. Vesc project. [Online]. Available: https://vesc-project.com/

[43] P. Lynn. Peter lynn kite sports. [Online]. Available: http://www.peterlynn.com/

[44] J. M. Jonkman, G. J. Hayman, B. J. Jonkman, and R. R. Damiani, *AeroDyn v15 Users Guide and Theory Manual*, NREL, Denver, Colorado. [Online]. Available: https://wind.nrel.gov/nwtc/docs/AeroDyn_Manual.pdf

[45] C. Ostowari and D. Naik, "Post-stall wind tunnel data for naca 44xx series airfoil sections," Solar Energy Research Institute, Golden, Colorado, USA, Tech. Rep., 1985.

[46] O. Tulloch, "Modelling and simulation studies of a rotary kite airborne wind energy (awe) system," 2015, CDT Mini Project Report.

Appendix A

AeroDyn Input Files

```
------- AERODYN  INPUT FILE ------------------------------------------------
Description line that will be printed in the output file and written to the screen.
======  General Options
================================================================================
False         Echo               - Echo the input to "<rootname>.AD.ech"?  (flag)
"default"     DTAero             - Time interval for aerodynamic calculations {or
"default"} (s)
          1   WakeMod            - Type of wake/induction model (switch) {0=none, 1
=BEMT}
          1   AFAeroMod          - Type of blade airfoil aerodynamics model (switch) {1
=steady model, 2=Beddoes-Leishman unsteady model} [must be 1 when linearizing]
          0   TwrPotent          - Type tower influence on wind based on potential flow
around the tower (switch) {0=none, 1=baseline potential flow, 2=potential flow…
False         TwrShadow          – Calculate tower influence on wind based on downstream
tower shadow? (flag)
False         TwrAero            - Calculate tower aerodynamic loads? (flag)
False         FrozenWake         - Assume frozen wake during linearization? (flag) [used
only when WakeMod=1 and when linearizing]
False         CavitCheck         - Perform cavitation check? (flag)
======  Environmental Conditions
================================================================================
      1.225   AirDens            - Air density (kg/m^3)
  1.460E-05   KinVisc            - Kinematic air viscosity (m^2/s)
      340.3   SpdSound           - Speed of sound (m/s)
     101325   Patm               - Atmospheric pressure (Pa) [used only when
CavitCheck=True]
       2000   Pvap               - Vapour pressure of fluid (Pa) [used only when
CavitCheck=True]
        0.6   FluidDepth         - Water depth above mid-hub height (m) [used only when
CavitCheck=True]
======  Blade-Element/Momentum Theory Options
================================================== [used only when WakeMod=1]
          1   SkewMod            - Type of skewed-wake correction model (switch) {1
=uncoupled, 2=Pitt/Peters, 3=coupled} [used only when WakeMod=1]
True          TipLoss            - Use the Prandtl tip-loss model? (flag) [used only
when WakeMod=1]
True          HubLoss            - Use the Prandtl hub-loss model? (flag) [used only
when WakeMod=1]
True          TanInd             - Include tangential induction in BEMT calculations?
(flag) [used only when WakeMod=1]
True          AIDrag             - Include the drag term in the axial-induction
calculation? (flag) [used only when WakeMod=1]
True          TIDrag             - Include the drag term in the tangential-induction
calculation? (flag) [used only when WakeMod=1 and TanInd=TRUE]
      5E-05   IndToler           - Convergence tolerance for BEMT nonlinear solve
residual equation {or “default”} (-) [used only when WakeMod=1]
        100   MaxIter            - Maximum number of iteration steps (-) [used only when
WakeMod=1]
======  Beddoes-Leishman Unsteady Airfoil Aerodynamics Options
==================================== [used only when AFAeroMod=2]
          1   UAMod              - Unsteady Aero Model Switch (switch) {1=Baseline model
(Original), 2=Gonzalez’s variant (changes in Cn,Cc,Cm), 3=Minemma/Pierce…
FALSE         FLookup            - Flag to indicate whether a lookup for f' will be
calculated (TRUE) or whether best-fit exponential equations will be used (FALSE);…
======  Airfoil Information
================================================================================
          1   InCol_Alfa         - The column in the airfoil tables that contains the
angle of attack (-)
          2   InCol_Cl           - The column in the airfoil tables that contains the
lift coefficient (-)
          3   InCol_Cd           - The column in the airfoil tables that contains the
drag coefficient (-)
          0   InCol_Cm           - The column in the airfoil tables that contains the
pitching-moment coefficient; use zero if there is no Cm column (-)
          0   InCol_Cpmin        - The column in the airfoil tables that contains the
Cpmin coefficient; use zero if there is no Cpmin column (-)
          1   NumAFfiles         - Number of airfoil files used (-)
"ad_airfoil_Daisy.inp"    AFNames            - Airfoil file names (NumAFfiles lines)
(quoted strings)
======  Rotor/Blade Properties
================================================================================
```

```
False          UseBlCm            - Include aerodynamic pitching moment in calculations?
(flag)
"ad_blade_Daisy.inp"    ADBlFile(1)        - Name of file containing distributed
aerodynamic properties for Blade #1 (-)
"ad_blade_Daisy.inp"    ADBlFile(2)        - Name of file containing distributed
aerodynamic properties for Blade #2 (-) [unused if NumBl < 2]
"ad_blade_Daisy.inp"    ADBlFile(3)        - Name of file containing distributed
aerodynamic properties for Blade #3 (-) [unused if NumBl < 3]
======  Tower Influence and Aerodynamics
========================================================== [used only when TwrInflnc/
=0, or TwrAero=True]
          5   NumTwrNds          - Number of tower nodes used in the analysis  (-) [used
only when TwrInflnc/=0, or TwrAero=True]
TwrElev        TwrDiam        TwrCd
(m)              (m)           (-)
0.0000000E+00  6.0000000E+00  0.0000000E+00
2.0000000E+01  5.5000000E+00  0.0000000E+00
4.0000000E+01  5.0000000E+00  0.0000000E+00
6.0000000E+01  4.5000000E+00  0.0000000E+00
8.0000000E+01  4.0000000E+00  0.0000000E+00
======  Outputs
================================================================================
False         SumPrint           - Generate a summary file listing input options and
interpolated properties to "<rootname>.AD.sum"?  (flag)
          4   NBlOuts            - Number of blade node outputs [0 - 9] (-)
          1,          4,         8,          10    BlOutNd             - Blade nodes
whose values will be output  (-)
          0   NTwOuts            - Number of tower node outputs [0 - 9]  (-)
          0   TwOutNd            - Tower nodes whose values will be output  (-)
              OutList            - The next line(s) contains a list of output
parameters.  See OutListParameters.xlsx for a listing of available output channels, (-)
"B1Azimuth, B2Azimuth, B3Azimuth"             ! azimuth anlge of blades 1, 2 and 3
"B1N1VRel, B1N2VRel, B1N3VRel, B1N4VRel"      ! relative wind velocity blade 1
"B2N1VRel, B2N2VRel, B2N3VRel, B2N4VRel"      ! relative wind velocity blade 2
"B3N1VRel, B3N2VRel, B3N3VRel, B3N4VRel"      ! relative wind velocity blade 3
"B1N1Alpha, B1N2Alpha, B1N3Alpha, B1N4Alpha" ! angle of attack balde 1
"B2N1Alpha, B2N2Alpha, B2N3Alpha, B2N4Alpha" ! angle of attack balde 2
"B3N1Alpha, B3N2Alpha, B3N3Alpha, B3N4Alpha" ! angle of attack balde 3
"B1N1Fx, B1N2Fx, B1N3Fx, B1N4Fx"              ! out of place plane force per unit length
blade 1
"B2N1Fx, B2N2Fx, B2N3Fx, B2N4Fx"              ! out of place plane force per unit length
blade 2
"B3N1Fx, B3N2Fx, B3N3Fx, B3N4Fx"              ! out of place plane force per unit length
blade 3
"B1N1Fy, B1N2Fy, B1N3Fy, B1N4Fy"              ! in place plane force per unit length
blade 1
"B2N1Fy, B2N2Fy, B2N3Fy, B2N4Fy"              ! in place plane force per unit length
blade 2
"B3N1Fy, B3N2Fy, B3N3Fy, B3N4Fy"              ! in place plane force per unit length
blade 3
"RtSpeed, RtSkew, RtAeroPwr"                  ! rotor speed, skew and aerodynamic power
"RtAeroFxh, RtAeroFyh, RtAeroFzh"             ! total rotor aerdynamic load in x, y, and
z direction
"RtAeroCp, RtAeroCq, RtAeroCt"                ! power, torque and thrust coefficient
END of input file (the word "END" must appear in the first 3 columns of this last
OutList line)
---------------------------------------------------------------------------------------
```

```
! "Prediction of Aerodynamic Characteristics of Ram-Air Parachutes, M. Ghoreyshi et al.
2016"
! "Clark Y-M15 Areofoil, Re = 0.2 million for AoA 0 - 30, scalled from example file
outside that"
! ------------------------------------------------------------------------------
"DEFAULT"     InterpOrd         ! Interpolation order to use for quasi-steady table
lookup {1=linear; 3=cubic spline; "default"} [default=3]
! ------------------------------------------------------------------------------
          1   NonDimArea        ! The non-dimensional area of the airfoil (area/chord^2)
(set to 1.0 if unsure or unneeded)
          0  NumCoords          ! The number of coordinates in the airfoil shape file
(including an extra coordinate for airfoil reference).  Set to zero if coordinates…
! ......... x-y coordinates are next if NumCoords > 0 .............
! x-y coordinate of airfoil reference
!  x/c        y/c
! ------------------------------------------------------------------------------
          1   NumTabs           ! Number of airfoil tables in this file.  Each table
must have lines for Re and Ctrl.
! ------------------------------------------------------------------------------
! data for table 1
! ------------------------------------------------------------------------------
        0.2   Re                ! Reynolds number in millions
          0   Ctrl              ! Control setting (must be 0 for current AirfoilInfo)
true          InclUAdata        ! Is unsteady aerodynamics data included in this table?
If TRUE, then include 30 UA coefficients below this line
!..................................... "Taken from example file, only used if
AFAeroMod = 2"
      -0.38   alpha0            ! 0-lift angle of attack, depends on airfoil.
       15.3   alpha1            ! Angle of attack at f=0.7, (approximately the stall
angle) for AOA>alpha0. (deg)
      -15.3   alpha2            ! Angle of attack at f=0.7, (approximately the stall
angle) for AOA<alpha0. (deg)
          1   eta_e             ! Recovery factor in the range [0.85 - 0.95] used only
for UAMOD=1, it is set to 1 in the code when flookup=True. (-)
    7.12499   C_nalpha          ! Slope of the 2D normal force coefficient curve.
(1/rad)
          2   T_f0              ! Initial value of the time constant associated with Df
in the expression of Df and f''. [default = 3]
          7   T_V0              ! Initial value of the time constant associated with the
vortex lift decay process; it is used in the expression of Cvn. It depends on…
        1.6   T_p               ! Boundary-layer,leading edge pressure gradient time
constant in the expression of Dp. It should be tuned based on airfoil experimental…
          9   T_VL              ! Initial value of the time constant associated with the
vortex advection process; it represents the non-dimensional time in semi-…
"Default"     b1                ! Constant in the expression of phi_alpha^c and phi_q^c.
This value is relatively insensitive for thin airfoils, but may be different…
"Default"     b2                ! Constant in the expression of phi_alpha^c and phi_q^c.
This value is relatively insensitive for thin airfoils, but may be different…
        0.5   b5                ! Constant in the expression of K'''_q,Cm_q^nc, and
k_m,q.  [from  experimental results, defaults to 5]
"Default"     A1                ! Constant in the expression of phi_alpha^c and phi_q^c.
This value is relatively insensitive for thin airfoils, but may be different…
"Default"     A2                ! Constant in the expression of phi_alpha^c and phi_q^c.
This value is relatively insensitive for thin airfoils, but may be different…
"Default"     A5                ! Constant in the expression of K'''_q,Cm_q^nc, and
k_m,q. [from experimental results, defaults to 1]
     18.269   S1                ! Constant in the f curve best-fit for alpha0<=AOA
<=alpha1; by definition it depends on the airfoil. [ignored if UAMod<>1]
    -11.324   S2                ! Constant in the f curve best-fit for         AOA>
alpha1; by definition it depends on the airfoil. [ignored if UAMod<>1]
     18.269   S3                ! Constant in the f curve best-fit for alpha2<=AOA<
alpha0; by definition it depends on the airfoil. [ignored if UAMod<>1]
    -11.324   S4                ! Constant in the f curve best-fit for         AOA<
alpha2; by definition it depends on the airfoil. [ignored if UAMod<>1]
     1.9408   Cn1               ! Critical value of C0n at leading edge separation. It
should be extracted from airfoil data at a given Mach and Reynolds number. It…
       -0.8   Cn2               ! As Cn1 for negative AOAs.
"Default"     St_sh             ! Strouhal's shedding frequency constant.  [default =
0.19]
     0.0016   Cd0               ! 2D drag coefficient value at 0-lift.
    -0.0328   Cm0               ! 2D pitching moment coefficient about 1/4-chord
```

```
location, at 0-lift, positive if nose up. [If the aerodynamics coefficients table does…
          0   k0                ! Constant in the \hat(x)_cp curve best-fit; = (\hat(x)
_AC-0.25).  [ignored if UAMod<>1]
          0   k1                ! Constant in the \hat(x)_cp curve best-fit.  [ignored
if UAMod<>1]
          0   k2                ! Constant in the \hat(x)_cp curve best-fit.  [ignored
if UAMod<>1]
          0   k3                ! Constant in the \hat(x)_cp curve best-fit.  [ignored
if UAMod<>1]
          0   k1_hat            ! Constant in the expression of Cc due to leading edge
vortex effects.  [ignored if UAMod<>1]
"Default"     x_cp_bar          ! Constant in the expression of \hat(x)_cp^v. [ignored
if UAMod<>1, default = 0.2]
"DEFAULT"     UACutout          ! Angle of attack above which unsteady aerodynamics are
disabled (deg). [Specifying the string "Default" sets UACutout to 45 degrees]
"DEFAULT"     filtCutOff        ! Cut-off frequency (-3 dB corner frequency) for low-
pass filtering the AoA input to UA, as well as the 1st and 2nd derivatives (Hz)…
!.....................................
! Table of aerodynamics coefficients
         56   NumAlf            ! Number of data lines in the following table
!    Alpha      Cl      Cd
!    (deg)      (-)     (-)
-180 0 0.05
-170 0.2 0.12
-160 0.3 0.32
-150 0.36 0.7
-140 0.4 1.05
-130 0.36 1.2
-120 0.3 1.32
-110 0.2 1.38
-100 0.1 1.42
-90 0 1.45
-80 -0.08 1.42
-70 -0.15 1.38
-60 -0.18 1.32
-50 -0.2 1.2
-45 -0.205 1.13
-40 -0.22 1.05
-35 -0.25 0.88
-30 -0.27 0.7
-25 -0.3 0.5
-20 -0.32 0.32
-15 -0.34 0.2
-10 -0.35 0.12
-5 -0.5 0.05
0 0.24 0.05
2 0.31 0.06
4 0.38 0.07
6 0.45 0.08
8 0.52 0.09
10 0.60 0.11
12 0.66 0.12
14 0.70 0.13
16 0.73 0.16
18 0.78 0.20
20 0.81 0.24
22 0.88 0.31
24 0.92 0.36
26 0.94 0.41
28 0.95 0.48
30 0.98 0.53
35 0.75 0.65
40 0.5 0.78
45 0.55 0.92
50 0.53 1.05
60 0.45 1.18
70 0.32 1.28
80 0.15 1.35
90 0 1.4
100 -0.1 1.35
110 -0.2 1.28
```

```
120 -0.3 1.12
130 -0.36 0.95
140 -0.4 0.68
150 -0.36 0.42
160 -0.3 0.3
170 -0.2 0.2
180 0 0.05
```

```
------- AERODYN v15.04.* BLADE DEFINITION INPUT FILE
------------------------------------
Description line for this file -- file corresponds to inputs in Test01_UAE_AeroDyn.dat
======  Blade Properties
====================================================================
   10               NumBlNds           - Number of blade nodes used in the analysis (-)
  BlSpn     BlCrvAC    BlSwpAC    BlCrvAng    BlTwist    BlChord    BlAFID
  (m)       (m)        (m)        (deg)       (deg)      (m)        (-)
 0.00       0.0        0.0        0.0         0.000      0.160       1
 0.1270     0.0        0.0        0.0         0.000      0.242       1
 0.2540     0.0        0.0        0.0         0.000      0.324       1
 0.3810     0.0        0.0        0.0         0.000      0.406       1
 0.5080     0.0        0.0        0.0         0.000      0.488       1
 0.6350     0.0        0.0        0.0         0.000      0.570       1
 0.7620     0.0        0.0        0.0         0.000      0.488       1
 0.8890     0.0        0.0        0.0         0.000      0.406       1
 1.0160     0.0        0.0        0.0         0.000      0.324       1
 1.1430     0.0        0.0        0.0         0.000      0.242       1
 1.2700     0.0        0.0        0.0         0.000      0.160       1
```

```
-----  AeroDyn Driver v1.00.x Input File  ------------------------------------
UAE Phase 3 turbine (BEM)
-----  Input Configuration  --------------------------------------------------
False         Echo            -  Echo input parameters to "<rootname>.ech"?
"ad_primary_Daisy.inp"    AD_InputFile    -  Name of the primary AeroDyn input file
-----  Turbine Data  ---------------------------------------------------------
          3   NumBlades       - Number of blades (-)
       1.16   HubRad          - Hub radius (m)
          3   HubHt           - Hub height (m)
          0   Overhang        - Overhang (m)
       24.2   ShftTilt        - Shaft tilt (deg)
          0   Precone         - Blade precone (deg)
-----  I/O Settings  ---------------------------------------------------------
"Daisy_Soft_7ms"      OutFileRoot     - Root name for any output files (use "" for .dvr
rootname) (-)
True          TabDel          - When generating formatted output (OutForm=True), make
output tab-delimited (fixed-width otherwise) (flag)
"ES10.3E2"    OutFmt          - Format used for text tabular output, excluding the time
channel.  Resulting field should be 10 characters. (quoted string)
True          Beep            - Beep on exit (flag)
-----  Combined-Case Analysis  -----------------------------------------------
        15   NumCases        - Number of cases to run
WndSpeed       ShearExp       RotSpd        Pitch            Yaw           dT
Tmax
(m/s)            (-)          (rpm)         (deg)           (deg)          (s)
(s)
7.0000000E+00  0.0000000E+00  1.0000000E+01  0.0000000E+00  0.0000000E+00  6.25000000E-
03  1.0000000E+01
7.0000000E+00  0.0000000E+00  2.0000000E+01  0.0000000E+00  0.0000000E+00  6.25000000E-
03  1.0000000E+01
7.0000000E+00  0.0000000E+00  3.0000000E+01  0.0000000E+00  0.0000000E+00  6.25000000E-
03  1.0000000E+01
7.0000000E+00  0.0000000E+00  4.0000000E+01  0.0000000E+00  0.0000000E+00  6.25000000E-
03  1.0000000E+01
7.0000000E+00  0.0000000E+00  5.0000000E+01  0.0000000E+00  0.0000000E+00  6.25000000E-
03  1.0000000E+01
7.0000000E+00  0.0000000E+00  6.0000000E+01  0.0000000E+00  0.0000000E+00  6.25000000E-
03  1.0000000E+01
7.0000000E+00  0.0000000E+00  7.0000000E+01  0.0000000E+00  0.0000000E+00  6.25000000E-
03  1.0000000E+01
7.0000000E+00  0.0000000E+00  8.0000000E+01  0.0000000E+00  0.0000000E+00  6.25000000E-
03  1.0000000E+01
7.0000000E+00  0.0000000E+00  9.0000000E+01  0.0000000E+00  0.0000000E+00  6.25000000E-
03  1.0000000E+01
7.0000000E+00  0.0000000E+00  1.0000000E+02  0.0000000E+00  0.0000000E+00  6.25000000E-
03  1.0000000E+01
7.0000000E+00  0.0000000E+00  1.1000000E+02  0.0000000E+00  0.0000000E+00  6.25000000E-
03  1.0000000E+01
7.0000000E+00  0.0000000E+00  1.2000000E+02  0.0000000E+00  0.0000000E+00  6.25000000E-
03  1.0000000E+01
7.0000000E+00  0.0000000E+00  1.3000000E+02  0.0000000E+00  0.0000000E+00  6.25000000E-
03  1.0000000E+01
7.0000000E+00  0.0000000E+00  1.4000000E+02  0.0000000E+00  0.0000000E+00  6.25000000E-
03  1.0000000E+01
7.0000000E+00  0.0000000E+00  1.5000000E+02  0.0000000E+00  0.0000000E+00  6.25000000E-
03  1.0000000E+01
```